

Fermi National Accelerator Laboratory

FN-353
8000.000

ANTIPROTON SOURCE FOR THE ACCELERATOR-STORAGE COMPLEX*

UNK - IHEP

T. Vsevolozskaja, B. Grishanov, Ya. Derbenev,
N. Dikansky, I. Meshkov, V. Parkhomchuk,
D. Pestrikov, G. Silvestrov, A. Strinsky

December 1981

*Translation of original preprint 80-182 (INP - Novosibirsk) of the same title in Russian. Translated and prepared by I. Meshkov, P. McIntyre, and W. Kells, Fermilab, June 1981.



Antiproton Source for the Accelerator-Storage Complex*

UNK - IHEP

T. Vsevolozskaja, B. Grishanov, Ya. Derbenev,
N. Dikansky, I. Meshkov, V. Parkhomchuk,
D. Pestrikov, G. Silvestrov, A. Skrinsky

ABSTRACT

In this article we present the design of the antiproton source for the UNK complex. Antiprotons are produced at 5.5 GeV/c momentum by targeting the proton beam of the U-70 synchrotron. They are decelerated to 400 MeV energy in a special decelerator synchrotron. The antiprotons are transferred to a cooler-accumulator ring where they are cooled and accumulated into an intense stack using the electron cooling method. The energy of 400 MeV is chosen for optimum electron cooling performance. An important feature of this cooler-accumulator is the very long cooling straight sections (2 x 100m), which become part of the focusing structure.

A scenario is presented for an accumulation rate of 5×10^7 \bar{p} /s. Some improvements of this scenario are discussed, and an accumulation rate of about 10^9 \bar{p} /s is predicted as attainable.

A luminosity of 3×10^{30} $\text{cm}^{-2} \text{s}^{-1}$ can be obtained for $p\bar{p}$ collisions with 10^{12} particles at 3 TeV per beam.

* Translation of original preprint 80-182 (INP - Novosibirsk) of the same title in Russian. Translated and prepared by I. Meshkov, P. McIntyre and W. Kells. Fermilab, June 1981.

TABLE OF CONTENTS

- I General Description of the \bar{p} -accumulator scheme
- II Antiproton Production
 - II.1 The targetry
- III Antiproton Accumulation rate
- IV The Electron Cooling
- V The Cooler-Accumulator
 - V.1 General scheme
 - V.2 Cooling section Antiproton orbit perturbations
 - V.3 Antiproton dynamics in the cooling section
 - V.4 Parameter choice. Accumulation rates.
 - V.5 Cooler Lattice
 - V.6 Antiproton beam lifetime in the cooler
 - V.7 Antiproton stacking. Luminosity.
 - V.8 Electron Cooling for Protons
- VI Synchrotron-Decelerator
 - VI.1 Lattice injection and extraction
 - VI.2 RF System
 - VI.3 Magnets
- VII Possibilities for antiproton source improvement
 - Methods for augmenting the accumulation rate
 - VII.1 Proton delay channels
 - VII.2 A buncher ring
 - VII.3 Multitargeting
 - VII.4 Efficiency increase by the use of all accelerated protons

TABLE OF CONTENTS

- VII.5 Increasing injection energy for U-70
- VII.6 Colliding region for UNK with low beta function
- VII.7 Electron cooling at interaction energy
- VIII Comparison of Antiproton Sources
- IX Antideuteron Accumulation

I. General Description of the \bar{p} -accumulator scheme

Electron cooling can be used for accumulation of intense antiproton beams of energy approximately 0.5 GeV or lower, if the available cooling time is on the order of tens of seconds ⁽¹⁾ and the electron cooler is to be constructed along proven lines (using \lesssim 250 kV beam potential, \lesssim few hundreds of amperes electron current, and beam kinetic energy recovery). However, the maximum antiproton yield for a proton energy of 70 GeV corresponds to an antiproton momentum of about 6 GeV/c. This situation dictates the use of an accumulation scheme with deceleration of antiprotons in a separate synchrotron and subsequently cooling them with electron cooling ⁽²⁾. As will be shown later, such a scheme is more effective than a first one, without deceleration^{*}, proposed by us a year ago ⁽³⁾.

The decelerator synchrotron has to have an acceptance which is large enough, and a special RF system for bunch "RF-rotation" (rotation of the longitudinal beam emittance in phase space to decrease the \bar{p} momentum spread) ⁽⁴⁾. The proton beam bunches, before extraction from U-70, will go through a similar (but time reversed) RF manipulation to shorten their longitudinal size.

* Note in translation. Recent experimental results, from Serphukov, on antiproton yields from heavy nucleus targets show the yield maximum to lie at lower antiproton momentum. ⁽¹⁵⁾ This fact brings closer to feasibility an electron accumulation scenario without post target deceleration.

The problem which predominates when a very intense and long electron beam is being used in a storage ring (accumulator) is the perturbation of \bar{p} beam motion by the electron beam space charge and its confining magnetic field. Therefore it seems unrealistic to combine, in the same lattice, both the functions of deceleration and accumulation. It appears possible to realize a good storage ring design incorporating such perturbations in the situation of a fixed parameter (D.C. ring, constant electron beam current density) accumulator (see section V)).

The general scenerio of antiproton accumulation is, in outline:

- 1). The acceleration of protons in the U-70 synchrotron up to an energy of 70 GeV.
- 2). "RF rotation" - the proton bunch length is shortened with 30th harmonic RF (30 bunches).
- 3). Extraction of the necessary numbers of bunches from U-70; focusing of these bunches on to a target; capture of antiprotons; and their injection into the accelerator synchrotron.
- 4). "RF-rotation" of antiproton bunches to decrease their momentum spread and then deceleration of antiprotons to the energy which is chosen for cooling.

The scheme for the antiproton source is shown in Fig. 1. It is capable of antiproton accumulation rates of about $5 \times 10^7 \bar{p}/s$, if the proton beam intensity (all 30 bunches in U-70) is 5×10^{13} p/cycle, which is too high a \bar{p} intensity for effective stochastic

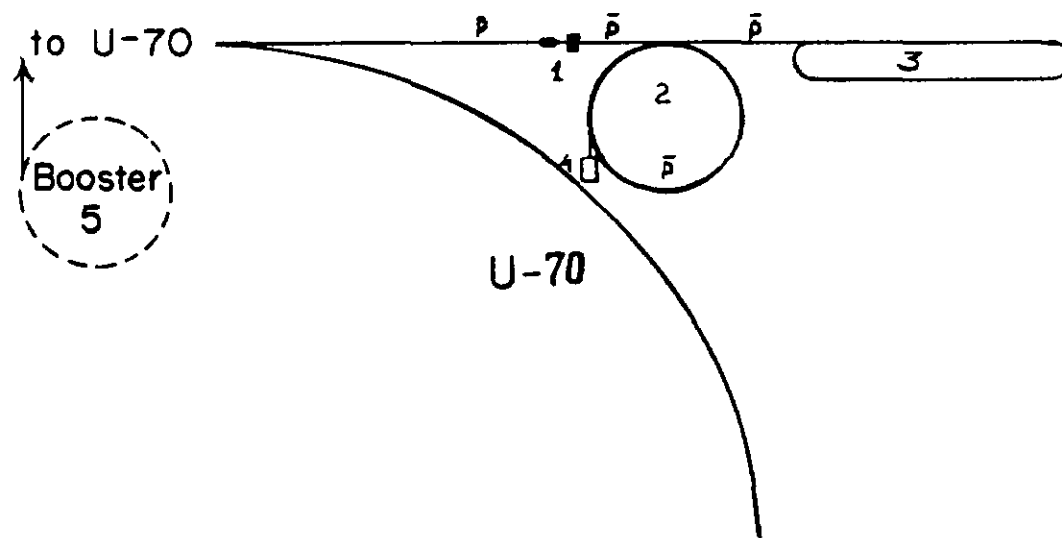


Fig. 1 The \bar{p} source plan.
 1. Target, 2. Synchrotron-decelerator,
 3. Cooler-accumulator,
 4. Special proton linear injector
 (see V.8), 5. U-70 Booster

cooling. But if the development of stochastic cooling proceeds so successfully, that its application becomes possible for intensities $\sim 10^9 \bar{p}/\text{cycle}$, then it could be used in the decelerator synchrotron for primary \bar{p} beam cooling. In this case the preparation of short bunches, with long intervals between, in U-70 will not be necessary; but it will be necessary to rebunch the proton beam before extraction into a single bunch whose length is less than or equal to the decelerator synchrotron circumference (see section IX).

The choice of scenario and parameters of the \bar{p} source depends very much on the parameters of proton beams in U-70. These are expected to be greatly altered by the new U-70 booster (under construction) so that choice of exact details of targetry and acceptance into the decelerator must wait for data of operation in this new mode.

II. ANTIPROTON PRODUCTION

The number of antiprotons accepted in the decelerator-synchrotron with a given emittance and beam momentum spread is defined by the antiproton production cross section $d\sigma/dp$ and targetry efficiency. The latter depends on the relation between the acceptance of the decelerator and emittance of the \bar{p} -beam, and on the inefficiency, due to absorption, for targets of finite length. The cross section $d\sigma/dp$ is related to $d^2\sigma/dpd\Omega$, which is the quantity usually measured in experiments, by the expression

$$\frac{d\sigma}{dp} \approx \frac{d^2\sigma}{dpd\Omega} \pi \langle \theta^2 \rangle$$

where $\langle \theta^2 \rangle =$ mean square of the antiproton production angle:

$$\langle \theta^2 \rangle = \frac{2\pi m_{\pi} c^2}{p^2} \quad (2.1)$$

with $p =$ antiproton momentum, and m, m_{π} the masses of the antiproton and pion. The capture coefficient,

$$k_{\bar{p}} \equiv N_{\bar{p}} / N_p$$

can be expressed as

$$k_{\bar{p}} = \frac{1}{\sigma_{in}} \frac{d\sigma}{dp} F \Delta p = \frac{2\pi m m_{\pi} c^2}{\sigma_{in}} F \cdot \frac{\Delta p}{p} \left(p \frac{d^3\sigma}{dp^3} \right) \quad (2.2)$$

where σ_{in} is the proton-nucleus inelastic cross section.

To achieve the maximum capture efficiency for acceptance ϵ , it is necessary to match the acceptance ellipses to the anti-proton distribution in phase space. If the values of proton cross section and antiproton absorption are approximately equal,

$$(\sigma_{in})_p \approx (\sigma_{in})_{\bar{p}} \equiv \bar{\sigma}_{in}$$

then expressions for the momenta of the \bar{p} -distribution may be written as

$$\begin{aligned} \langle r^2 \rangle &= \frac{1}{3} \langle \theta^2 \rangle \ell^2 \\ \langle r\theta \rangle &= \frac{1}{2} \langle \theta^2 \rangle \ell \end{aligned} \quad (2.3)$$

The effective values of \bar{p} beam emittance $\epsilon_{\bar{p}}$ and beta function $\beta_{\bar{p}}$ at the waist, which is located at the center of the target, are in this case,

$$\begin{aligned} \epsilon_{\bar{p}} &= \sqrt{\langle r^2 \rangle \langle \theta^2 \rangle - \langle r\theta \rangle^2} \approx \frac{\langle \theta^2 \rangle \ell}{2\sqrt{3}} \\ \beta_{\bar{p}} &= \epsilon_{\bar{p}} / \langle \theta^2 \rangle \approx \frac{\ell}{2\sqrt{3}} \end{aligned} \quad (2.4)$$

As an effective emittance, $\epsilon_{\bar{p}}^0$, of \bar{p} -production we may take the emittance which would be obtained from a target of length equal to the absorption length λ (this target length corresponds to roughly the maximum \bar{p} production):

$$\epsilon_{\bar{p}}^0 = \frac{\langle \theta^2 \rangle \lambda}{2\sqrt{3}} \quad (2.5)$$

If the acceptance, ε , is small in comparison with $\varepsilon \frac{0}{\bar{p}}$ ($\varepsilon \ll \varepsilon \frac{0}{\bar{p}}$), the acceptance beta-function β_{ac} is equal to $\beta_{\bar{p}}$ (Eq. 2.4), and the target length has the optimum value, $\ell = \ell_{opt}$; then an analytic estimation of capture efficiency gives:

$$\begin{aligned} F_{opt} &= \frac{8}{3} \frac{\varepsilon}{\langle \theta^2 \rangle (\lambda + \ell_{opt})} e^{-\ell_{opt}/\lambda} = \\ &= \frac{8}{3} \frac{\varepsilon}{\langle \theta^2 \rangle \lambda} \chi \end{aligned} \quad (2.6)$$

The value ℓ_{opt} for this case is

$$\ell_{opt} \approx 1.28 \lambda \sqrt{\frac{\varepsilon}{\langle \theta^2 \rangle \lambda} + \frac{3}{8} \frac{r_0^2}{\varepsilon \lambda}} \quad (2.7)$$

where r_0 is the proton beam radius on target. The coefficient

$$\chi \equiv \frac{e^{-x}}{1+x}, \quad x \equiv \frac{\ell_{opt}}{\lambda}$$

is equal to one if $\varepsilon/\varepsilon \frac{0}{\bar{p}} \rightarrow 0$, $r_0 = 0$, and changes slowly in the region of interest to us. This means that the dependence of the efficiency F on acceptance ε and on \bar{p} -momentum is described mainly by the factor $\varepsilon/\lambda \langle \theta^2 \rangle$.

For small values of ε ($\sim 10^{-2} \varepsilon \frac{0}{\bar{p}}$) the condition of equality $\beta_{ac} = \beta_{\bar{p}}$ is very far from optimum. The simultaneous optimization of β_{ac} and ℓ gives

$$\beta_{\text{opt}} = \frac{\lambda}{\pi} \frac{R^{2/3}}{1 - \frac{4}{3\pi} R^{1/3}} \quad , \quad (2.8)$$

$$\ell_{\text{opt}} = \frac{2\lambda}{\pi} \frac{R^{1/3}}{\left(1 - \frac{4}{3\pi} R^{1/3}\right)^2} \quad ,$$

$$F_{\text{max}} = \frac{4\varepsilon}{\langle\theta^2\rangle\lambda} \left(1 - \frac{4}{3\pi} R^{1/3}\right)^3 e^{-\ell_{\text{opt}}/\lambda} \quad , \quad (2.9)$$

where

$$R = \frac{\pi^2}{6} \left(\frac{\varepsilon}{\langle\theta^2\rangle\lambda} + \frac{3}{8} \frac{r_0^2}{\varepsilon\lambda} \right) \quad .$$

When $R \rightarrow 0$, the value of F_{max} differs from F (given by 2.6) only by a factor 1.5, but already for $R \sim 10^{-2}$ this difference is smaller than 10%. The condition of "thinness" of the proton beam follows from (2.7) and (2.9):

$$r_0^2 \ll \frac{8}{3} \frac{\varepsilon^2}{\langle\theta^2\rangle} \quad (2.10)$$

The analytic estimations of capture efficiency were made not taking into account the difference between proton and antiproton absorption lengths ($\lambda_p \approx 1.4 \lambda_{\bar{p}}$ for light nuclei and \bar{p} -momentum ~ 6 GeV/c), multiple scattering of antiprotons in the target, and the angular divergence of the proton beam due to its finite emittance. These factors were taken into account in computer simulations, which were done using Monte Carlo methods (Fig. 3,4).

The dependence of the efficiency F on proton beam size r_0 and \bar{p} -capture angle θ_m (or β_{ac}) defines the parameters of the focussing and collecting lenses. If the proton beam is "thin" (2.10), the

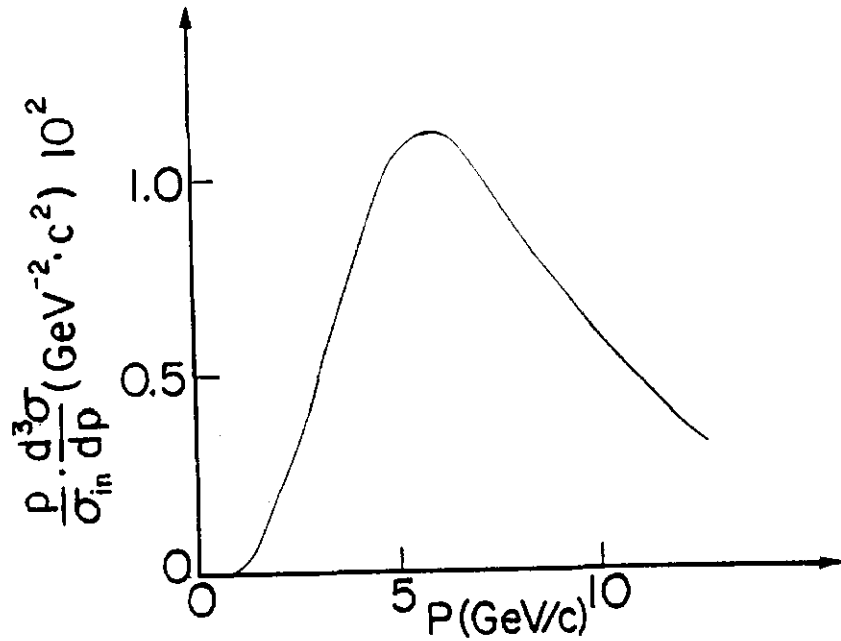


Fig. 2 Cross section of antiproton production per interacting proton for 70 GeV proton energy (result of Ref^{5,6} with symmetric reflection of values about $Y_F, pp = 0$).

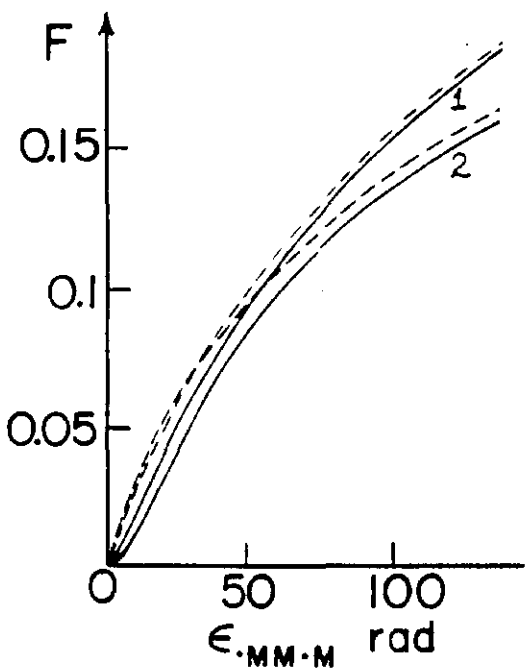


Fig. 3 Dependence of F on ϵ .
 Proton momentum, 76 GeV/c
 \bar{p} momentum, 6 GeV/c
 proton beam radius in target:
 $r_0 = 0$ (-----)
 $r_0 = 0.045$ (————)

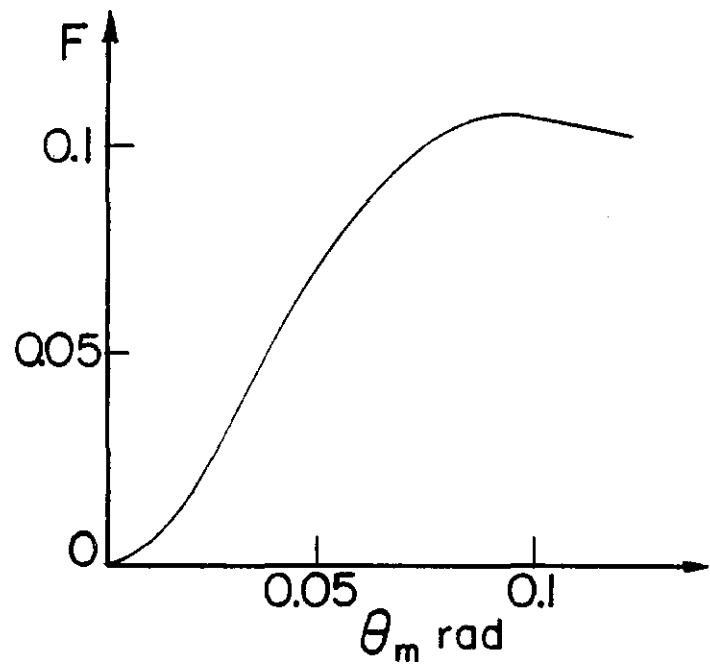


Fig. 4 Dependence of F on \bar{p} capture angle θ_m . Target length has its optimum value, and $\epsilon = 70 \text{ mm} \cdot \text{mrad}$.

dependence of F on r_0 is very weak. So, for the case of $\epsilon = 70$ mm mrad the values of efficiency F for $r_0 = 0$ and $r_0 = 0.5$ mm differ only by 7%. If $r_0 \rightarrow 1$ mm this difference is proportional to r_0^2 , and if $r_0^2 \gg \epsilon^2 / \langle \theta^2 \rangle$ the efficiency F decreases as r_0^{-2} .

II.1 THE TARGET

The \bar{p} -production system consists of a target and two lenses - one for focusing of protons and another for antiproton collection. For $\epsilon = 70$ mm mrad the required proton beam size on the target is $r_0 \approx 0.5 \div 1$ mm, which means, that for a proton emittance of 2 mm mrad, it is necessary to have axial symmetric focusing with a divergence cone of $2 \div 4 \times 10^{-5}$ sterad. In principle, such parameters for proton energy of 70 GeV, could be achieved with a quadrupole lens. The parameters can be readily achieved with a lithium lens, whose magnetic field is 100 KG, diameter is 5 mm and length is 10 cm. For antiproton collection from the target it is necessary to design a lithium lens which is able to collect antiprotons within a linear angle $\theta \approx 0.1$ rad. (solid angle 0.03 sterad). This has a magnetic field of 170 KG, a diameter of 2 cm, and a lens length of 15 cm.

III. ANTIPROTON ACCUMULATION RATE

The rate of antiproton accumulation is obviously given by the expression

$$\dot{N}_{\bar{p}} = k_{\bar{p}} N_p / \tau_c, \quad (3.1)$$

where N_p is the number of protons for the extracted beam, τ_c is the cycle duration of the entire source system, and $k_{\bar{p}}$ is the capture

coefficient (2.2). The choice of injection energy for the decelerator ($p \sim 6$ GeV/c) is given by the dependence on energy of the cross section per phase space volume d^3p/p , which is invariant under adiabatic deceleration. This volume consists of the factor

$$F \cdot \frac{\Delta p}{p} \propto \epsilon p^2 \frac{\Delta p}{p}$$

Its value is defined by the cooler and decelerator parameters, when the latter is taken at the cooling energy.

After RF-rotation and deceleration (section I, point 4) the antiproton momentum spread has the value

$$\left(\frac{\Delta p}{p} \right)_{\text{cool}} = \frac{n_b \ell_b}{2\pi R_o} \frac{p_t}{p_{\text{cool}}} \left(\frac{\Delta p}{p} \right)_t, \quad (3.2)$$

where indicies "t" and "cool" refer to values before and after rotation and deceleration, respectively. n_b is the number of antiproton bunches, and R_o is the average radius of the decelerator.

The antiproton emittance increases during deceleration

$$\epsilon_{\text{cool}} = \epsilon_b \frac{p_t}{p_{\text{cool}}} \quad (3.3)$$

The value of which, coolable in τ_c , fixes the value of the efficiency F which, in turn, determines the accumulation rate (see (3.1) and (2.2)).

For our scenario parameters it is convenient to use the approximate analytic expressions for F (2.6). Then, taking into account (2.1), (3.2), (3.3), and (2.2), we find

$$\dot{N}_{\bar{p}} = 10 \left(\frac{P}{\sigma_{in}} \frac{d^3\sigma}{dp^3} \right) P_{cool}^2 \left(\frac{\ell_{opt}}{\lambda} \right) \frac{\theta_{||} \theta_{\perp}^2}{\tau_c} \frac{N_b}{\ell_b} \beta_{eff} 2\pi R_o \quad (3.4)$$

where

$$\theta_{||} = 1/2 (\Delta p / p) \quad \text{and} \quad \theta_{\perp} = (\Delta p / p)$$

are the relative longitudinal and transverse momentum spreads of the cooled antiprotons; N_b the number of antiprotons per bunch; and β_{eff} the effective value of beta-function on the cooling region (see 5.24 and 5.25 below).

In section IV it will be shown (see (4.6)) that the parameter

$$\theta_{||} \theta_{\perp}^2 \propto \frac{j_e \tau_c}{\beta^4 \gamma^4} \quad (3.5)$$

where j_e is the electron current density. Due to this fact several remarkable characteristics of the accumulation rate $\dot{N}_{\bar{p}}$ follow from (3.4): it does not depend on the cycle duration τ_c or number of antiproton bunches n_b ; it is proportional to the line density of each proton bunch, N_b/ℓ_b ; and, if the electron current density is given, it decreases with energy as $(\beta^2\gamma^2)^{-1}$. That is,

$$\dot{N}_{\bar{p}} = A \left(\frac{p}{\sigma_{in}} \frac{d^3\sigma}{dp^3} \right) \frac{j_e}{\beta^2\gamma^2} \frac{N_b}{\ell_b} 2\pi R_o \quad (3.3a)$$

where A is a coefficient, independent of the cooler parameters.*

*Note, in translation: typically the maximum current density which could be achieved, is proportional to $\beta^3\gamma^3$ (see also Section V.3); this shows, once more, that the choice of cooling energy is essentially a question of reasonable engineering limits for the electron system high voltage supplies.

The calculation of \bar{p} -accumulation rate for large \bar{p} -emittances has to take into account the efficiency F , which is represented in Fig. 3:

$$\begin{aligned} \dot{N}_{\bar{p}} &= 2\pi M M_{\pi} c^2 \left(\frac{p}{\sigma_{in}} \cdot \frac{d^3\sigma}{dp^3} \right) F \left(\frac{\Delta p}{p} \right)_t \cdot \frac{N_{\bar{p}}}{\tau_c} \\ &= 0.8 \left(\frac{p}{\sigma_{in}} \cdot \frac{d^3\sigma}{dp^3} \right) F \left(\frac{\Delta p}{p} \right)_t \frac{N_{\bar{p}}}{\tau_c} \end{aligned} \quad (3.6)$$

In this last expression the parameter $(p/\sigma_{in}) (d^3\sigma/dp^3)$ is to be in $(\text{GeV}/c)^2$.

IV. THE ELECTRON COOLING

The cooling rate is defined by a friction force which, in the \bar{p} rest frame, is

$$\bar{F} = - \frac{4\pi n_e' e^4}{m} L_c \cdot \frac{V_{\bar{p}}}{V_{\bar{p}}^3} \quad (4.1)$$

where n_e' is the electron density; " L_c " is the Coulomb logarithm; e, m are the charge and mass of the electron. This expression contains only antiproton velocities $V_{\bar{p}}$, because, for initial cooling, it is much bigger than the electron velocities. The Coulomb logarithm in (4.1) is equal to:

$$L_c = \ln \frac{2m V_{\bar{p}}^2}{e^2 \rho_{\max}}$$

where

$$\rho_{\max} = \beta \theta_e \sqrt{4\pi n_e' r_e}$$

is the Debye radius, where θ_e is the angular spread of the electron beam, $r_e \equiv e^2/mc^2$ is the classical electron radius. If we take $V_{\bar{p}}/V_s \sim \theta_e \sim 3 \times 10^{-3}$ (V_s = the average \bar{p} velocity in the Lab frame), then one has

$$\text{Log } \sim 15 \quad (4.2)$$

It follows from (4.1) that during a time duration τ_e the velocity spread $V_{\bar{p}}$ will be cooled, such that

$$V_{\bar{p}.max}^3 = \frac{180\pi n_e' e^4 \eta \tau_e}{Mm} \quad (4.3)$$

or, in the laboratory frame,

$$\theta_{\perp}^2 + (\theta_{11}^2 / \gamma^2) \equiv \theta_0^2 = \left[\frac{180\pi n_e r_e r_p c \tau_e \eta}{\beta^3 \gamma^5} \right]^{2/3} \quad (4.4)$$

Here, r_e , r_p are the classical electron and proton radii; η is the fraction of circumference occupied by the electron beam, $\beta = V_s/c$,

$\gamma^{-2} = 1 - \beta^2$; and n_e is the lab frame electron density.

The \bar{p} -accumulation rate (3.4) is proportional to $\theta_{11} \theta_{\perp}^2$, which has a maximum value, for (see 4.4)

$$\theta_{11} = \gamma \theta_0 / \sqrt{3} \quad \theta_{\perp} = \sqrt{\frac{2}{3}} \theta_0 \quad (4.5)$$

of

$$(\theta_{11} \theta_{\perp}^2)_{max} \sim 220 \frac{r_e r_p c \eta n_e \tau_e}{\beta^3 \gamma^4} \quad (4.6)$$

The substitution of (4.6) in (3.4) shows that the accumulation rate depends on energy as $j_e/\beta^2\gamma^2$, where j_e is the electron beam current density.

V. THE COOLER-ACCUMULATOR

V.1 General Scheme

The influence on the heavy particle motion due to the fields of the electron beam and the cooling system is a major problem for application of electron cooling. In the scenario which is proposed here the influence of these fields is included in the focusing action of the storage ring lattice. This allows much larger electron current, such that the betatron tune shift, which is produced by the cooling system, has a value $\Delta\nu \sim 1$. At the same time it is necessary to compensate the electric field of the electron beam by the field of ions which are allowed to be trapped in the electron beam for this purpose. This compensation, first, limits the electron's velocity spread primarily to the transverse direction with respect to the beam axis and, second, enhances the stability of \bar{p} -orbits in the storage ring (see (5.12, 13) below).

The cooler-accumulator consists of two half rings and two long straight sections, in which the solenoids with the electron beams are located (Fig. 5). It is possible to pass the same electron beam through both straight sections (Fig. 5). In this case the electron source (a gun) and collector have a common high potential. In a scheme with separated beams there would be two of these high voltage devices, and the gun for the first beam would be tied, at high potential, with the collector of the second beam, and vice-versa.

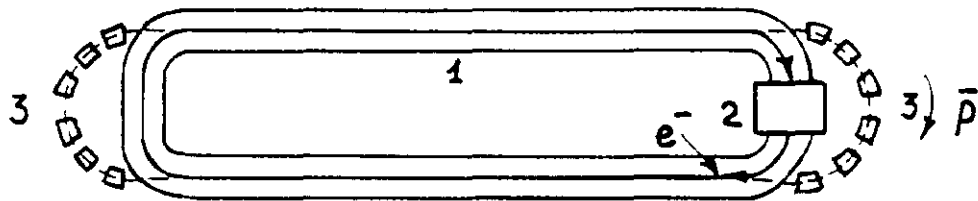


Fig. 5 The cooler-accumulator plan.
1. Solenoid with longitudinal magnetic field.
2. Electron gun and collector
3. Antiproton bending magnet channel.

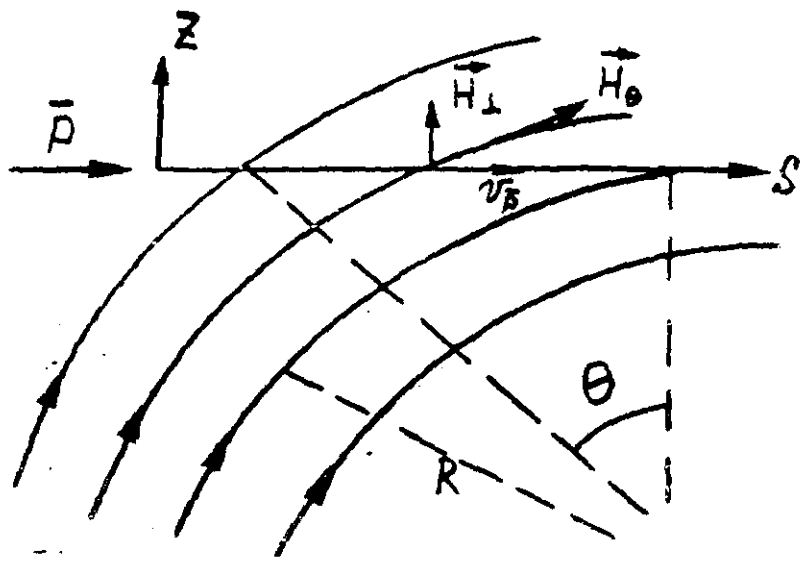
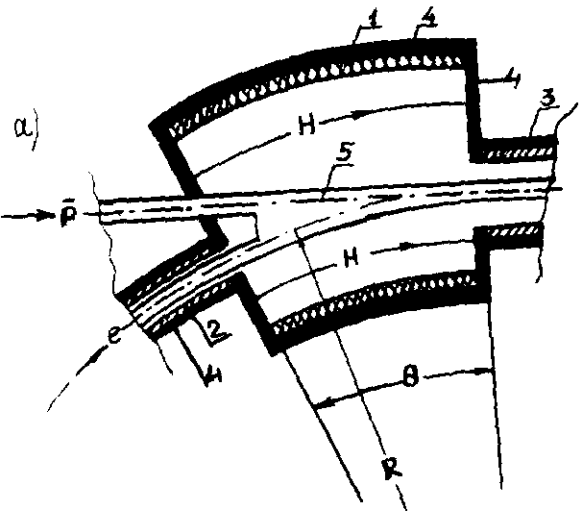


Fig. 6 Trajectory of antiprotons and geometry of the magnetic fields in the cooler toroid region.

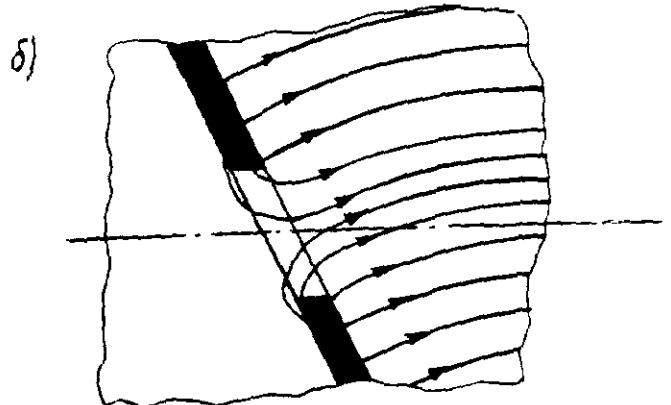
Fig. 7 Injection of antiprotons and electrons into the cooling section.

A. Layout of electron guide field and accompanying flux return steel

1. Large toroidal solenoid
2. Small toroidal solenoid
3. Long straight solenoid
4. Flux return
5. Vacuum Chamber



B. Magnetic flux lines near interface



V.2 Cooling Section Antiproton Orbit Perturbations

Antiprotons receive a kick whenever they enter or exit the cooling section. This kick is transverse to the proton beam axis and results from the transverse components of the magnetic field of the electron cooling system. These components are from two sources.

The first one is due to the transition at the ends of the cooling region from solenoidal to toroidal field (Fig. 6,7), where the antiprotons obtain a kick directed transverse to the toroid plane. Because the toroidal field decreases along the toroid radius of curvature as R^{-1} , the antiproton bending angle and antiproton displacement after crossing these areas are⁽⁷⁾

$$\Delta\left(\frac{dx}{ds}\right) = -\frac{e}{pc} \int_0^{\Delta s} ds H_{\perp} = \frac{eHR}{pc} \ln(\cos\theta) \quad (5.1)$$

$$\Delta x = -\frac{eHR^2}{pc} (\tan\theta - \theta) \quad (5.2)$$

where $p = \beta\gamma Mc$, the antiproton momentum; H , the magnetic field value in the straight section; R , the radius of curvature of field lines where the field value is equal to H ; θ the azimuthal length of the toroidal field region which the antiprotons traverse. At the exit of the cooling region this transverse component changes sign. For antiprotons, with energy 400 MeV, and for $H = 2\text{kG}$, $\ell = 3\text{m}$, $\theta = 20^\circ$ the values of (5.1,2) are

$$\Delta\left(\frac{dx}{ds}\right) = 1.2 \times 10^{-2} \quad ; \quad \Delta x = 8.4 \text{ mm}$$

Certainly, such an angle is prohibitively large. However these disturbances can be compensated by correction dipole fields, as for instance, proposed in Ref. 7.

The second source of transverse field components is the entrance (exit) hole for antiprotons. The simplest hole design is shown in Fig. 7⁽⁷⁾. Near such a hole there is always "outgoing" magnetic flux. In this case (Fig. 7b) it terminates on the magnetic flux return steel, and, as a result, transverse field components appear. If the hole is round, the field geometry is approximately axial-symmetric, with the symmetry axis fixed by the hole position. As a result, the kick of transverse field components is in the azimuthal (for this axis) direction, like that of a particle entering a cylindrical solenoid. The extent of this perturbing field is short if $pc \gg eHd$, where d is the hole diameter. Then the antiproton displacement in this region is negligible, but the angular deflection is large:

$$\begin{aligned} x'(s=0) &= x'_{in} + \frac{\omega_H}{2} z'_{in} \\ z'(s=0) &= z'_{in} - \frac{\omega_H}{2} x'_{in} \end{aligned} \tag{5.3}$$

where x, z, s are the usual beam coordinates, $()' = d/ds$;

$$\omega_H = \frac{eH}{pc} \quad [cm^{-1}] \tag{5.4}$$

and the index "in" is used for initial parameter values, before the boundary field crossing. Similar expressions can be written for the exit region of the cooling section:

$$\begin{aligned} x'_{out} &= x'(L) - \frac{\omega_H}{2} z(L) \\ z'_{out} &= z'(L) + \frac{\omega_H}{2} x(L) \end{aligned} \quad (5.5)$$

These results are well known from electron optics (so called "Bush's Theorem"). Note that, if the hole in the flux return is made a slit, the boundary field becomes two dimensional (a "cylindrical lens", and the boundary field kick is oriented along the long side of the slit. The expressions (5.3) change, but coupling of the x-z antiproton motion in the solenoid takes place for this case too.

V.3 Antiproton Beam Dynamics in the Cooling Section.

The equations of antiproton motion in a straight section with longitudinal magnetic field and electron beam field are

$$\begin{aligned} x'' &= \omega_H z' - \omega_e^2 x \\ z'' &= -\omega_H x' - \omega_e^2 z \end{aligned} \quad (5.6)$$

where the transverse coordinates x, z and longitudinal on s represent a right handed three dimensional coordinate system.

$$\omega_e^2 = - \frac{F}{\beta^3 \gamma} \frac{2\pi e j_e}{M c^3} \quad (5.7)$$

$$F = 1 - \beta^2 - \mathcal{K} \quad , \quad \mathcal{K} = n_i / n_e \quad (5.8)$$

where ω_H , ω_e are the "space" frequencies (cm^{-1}); e is the electron charge, j_e is the electron current density, M is the antiproton

mass, n_i is the density of ions in the electron beam, whose particle density is n_e .

It is more convenient to use complex functions for the transverse equations,

$$\xi(s) = x + iz \quad \xi' = x' + iz'$$

These coupled equations (5.6) could be combined in one,

$$\xi'' + i\omega_H \xi' + \omega_e^2 \xi = 0 \quad (5.9)$$

whose solution is of the form

$$\xi(s) = A e^{i\omega_1 s} + B e^{i\omega_2 s} \quad (5.10)$$

where

$$\omega_{1,2} = -\frac{\omega_H}{2} \pm \sqrt{\left(\frac{\omega_H}{2}\right)^2 + \omega_e^2} \equiv -\frac{\omega_H}{2} \pm \omega_c \quad (5.11)$$

It follows from (5.11) that for an unneutralized beam ($\gamma = 0$) the antiproton motion will be stable if $\omega_0^2 > 0$, or

$$j_e < \frac{Mc^3}{e} \frac{\beta^3}{8\pi} \left(\frac{eH}{pc}\right)^2 \quad (5.12)$$

If necessary, for larger current densities, the electric field of the electron beam can be compensated by ions, so for any j_e

$$\tilde{F} < 0, \quad \omega_e^2 > 0. \quad (5.13)$$

Using the initial condition (ξ_c, ξ'_c) to determine the constants A and B in (5.10) one can derive the transfer matrix for the cooling region:

$$\begin{pmatrix} \xi \\ \xi' \end{pmatrix}_s = e^{-i\frac{\omega_H S}{2}} \begin{pmatrix} \cos \omega_c S + i\frac{\omega_H}{2\omega_c} \sin \omega_c S & \frac{\sin \omega_c S}{\omega_c} \\ -\omega_c^2 \frac{\sin \omega_c S}{\omega_c} & \cos \omega_c S - i\frac{\omega_H}{2\omega_c} \sin \omega_c S \end{pmatrix} \begin{pmatrix} \xi \\ \xi' \end{pmatrix}_c \quad (5.14)$$

The complete transfer matrix for the cooling system can be obtained if we take into account the field kicks at the entrance and exit (see (5.3) and (5.5)):

$$\begin{pmatrix} \xi \\ \xi' \end{pmatrix}_c = \begin{pmatrix} 1 & 0 \\ -i\frac{\omega_H}{2} & 1 \end{pmatrix} \begin{pmatrix} \xi \\ \xi' \end{pmatrix}_{in} ; \quad \begin{pmatrix} \xi \\ \xi' \end{pmatrix}_{out} = \begin{pmatrix} 1 & 0 \\ i\frac{\omega_H}{2} & 1 \end{pmatrix} \begin{pmatrix} \xi \\ \xi' \end{pmatrix}_L \quad (5.15)$$

matrix multiplication then yields,

$$\begin{pmatrix} \xi \\ \xi' \end{pmatrix}_{out} = M_{cool} \begin{pmatrix} \xi \\ \xi' \end{pmatrix}_{in} \quad (5.16)$$

$$M_{cool} = e^{-i\frac{\omega_H L}{2}} \begin{pmatrix} \cos \omega_c L & \frac{\sin \omega_c L}{\omega_c} \\ -\omega_c \sin \omega_c L & \cos \omega_c L \end{pmatrix}$$

If the cyclotron phase shift $\omega_H L$ for the section length is equal to

$$\omega_H L = 2\pi m \quad m = 0, 1, 2, \dots \quad (5.17)$$

The exponential term in (5.16) is equal to $(-1)^m$, and the matrix M_{cool} is real. This indicates the absence of transverse oscillation coupling in each half ring of the accumulator. Alternately, such a coupling is produced by the solenoid field.

If, for any reason, condition (5.17) cannot be satisfied, (for example, if it is necessary to work with lower or higher magnetic field than was calculated from (5.17)), coupling can still be excluded if one installs two additional solenoids in front of and behind the cooling section. In this case, when the cyclotron phase shift for the integral longitudinal magnetic field is equal to $2\pi m$ the coupling disappears also, as a consequence of the matrix structure (5.16).

The transfer matrix for a solenoid without the electron beam can be obtained from (5.16), if

$$\dot{j}_e = 0, \quad \omega_c = \frac{\omega_H}{2} = \frac{\omega}{2} \quad (5.18)$$

then

$$M_{\text{sol}} = e^{\frac{i\omega l}{2}} \begin{bmatrix} \cos \frac{\omega l}{2} & \frac{2 \sin \frac{\omega l}{2}}{\omega} \\ -\frac{\omega}{2} \sin \frac{\omega l}{2} & \cos \frac{\omega l}{2} \end{bmatrix}. \quad (5.19)$$

After multiplication by matrices for these compensating solenoids one obtains

$$M = e^{i\psi} * |M_{sok2}| * |M_{cool}| * |M_{sok1}| \quad (5.20)$$

$$\psi = \sum \frac{\omega_n l_n}{\lambda} = \frac{e}{2pc} \int ds H_{II}(s).$$

Here, the symbol $| |$ means modulus of matrices (5.16, 19), i.e. matrices without phase factors. It is obvious, that if

$$\psi = 2\pi m \quad , \quad (5.21)$$

the matrix M is real and coupling disappears. Below, the case when condition (5.17) is satisfied, will be considered.

Now, let us investigate the particle motion in the cooling ring with a straight section, such as described here. The transfer matrix for a half ring can be written

$$M = \begin{bmatrix} \cos \mu & \beta \sin \mu \\ -\frac{\sin \mu}{\beta} & \cos \mu \end{bmatrix} \quad (5.22)$$

where β is the beta function value ($\beta_x = \beta_z = \beta$) at the cooling section entrance (exit), μ is the betatron phase shift in the half ring. The transfer matrix for a periodic element which is equal, in our cooler, to a cooling section plus one half of the ring, can be obtained by multiplication of (5.22) and (5.16). The following equation for betatron frequencies follows from this transfer matrix:

$$\cos \mu_t = \cos \omega_c L \cos \mu - \frac{1}{2} \left(\omega_c \beta + \frac{1}{\omega_c \beta} \right) \sin \omega_c L \sin \mu \quad (5.23)$$

$$\beta_t = \frac{\sin \omega_c L \cos \mu + \beta \omega_c \cos \omega_c L \sin \mu}{\omega_c \sin \mu_t} \quad (5.24)$$

$$\beta_t' = \left(\omega_c \beta - \frac{1}{\omega_c \beta} \right) \frac{\sin \omega_c L \sin \mu}{\sin \mu_t}$$

Note, that the condition of betatron oscillation stability

$$\left| \cos \mu_T \right| < 1$$

can be satisfied most simply if one takes (see (5.23))

$$\beta = \frac{1}{\omega_c} \quad (5.25)$$

In this case

$$\mu_t = \mu + \omega_c L, \quad \beta_t = \frac{1}{\omega_c}, \quad \beta_t' = 0. \quad (5.26)$$

One example of a stability region for betatron oscillations in the chosen cooler lattice (see section V 5) is shown in Fig. 7a.

The condition (5.25) is convenient from the point of view of antiproton beam sizes in the cooling region. For this value of beta function the beam cross section is a circle with constant radius:

$$a = a_{in} = \sqrt{\epsilon / \omega_c} \quad (5.27)$$

where ϵ is the \bar{p} beam emittance. Following from the expressions for \bar{p} coordinates inside the solution, multiplication of (5.17) by (5.15) gives

$$\xi(s) = \left(\xi_{in} \cos \psi_0 + \xi_{in} \frac{\sin \psi_0}{\omega_c} \right) e^{-i\psi_H} \quad (5.28)$$

$$\psi_0 = \omega_c s \quad \psi_H = \frac{1}{2} \omega_H s$$

And if $\beta = 1/\omega_0$, then

$$|\xi(s)|^2 = |\xi_{in}|^2 = a_{in}^2 \quad (5.29)$$

Therefore, the \bar{p} -beam radius inside the solenoid does not exceed the entrance beam size a , and the antiproton angular spread does not exceed

$$\theta_{\perp} \leq \omega_c a \quad (5.30)$$

If it is necessary, for any reason, to exclude the perturbing influence of the cooling section on the antiproton motion, this can be achieved by the proper choice of electron current density, so that the transfer matrix (5.16) becomes unity (i.e. $\omega_0 L = k\pi$), or with (5.17),

$$\omega_e = \frac{m\pi}{L} \sqrt{k^2 - 1} \quad (5.31)$$

Then,

$$M_{cool} = (-1)^{m(k+1)} \quad (5.32)$$

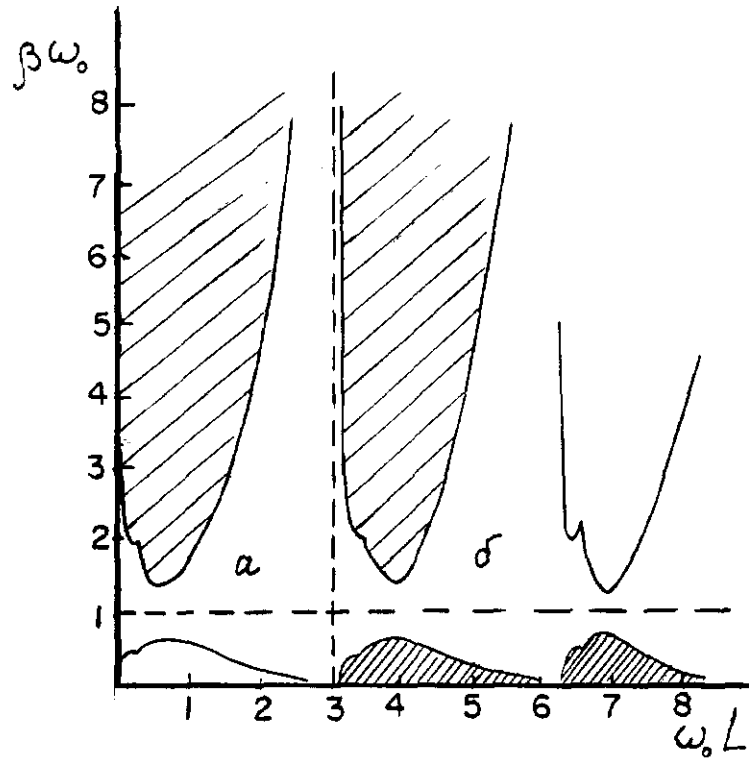


Fig. 7 Regions of betatron oscillation stability, as given in section (V.5). β is the beta function at the cooling section entrance; L the section length; ω_0 is given by (5.11). Instability regions are shaded. a is the unneutralized case; b the neutralized one.

For minimal values of m and k the parameters of the cooling section have the following values:

$$m = 1, \quad k = 2, \quad M = (-1)$$

$$\omega_{Hmin} = \omega_{\phi min} = \frac{2\pi}{L} \quad ; \quad H_{min} = \frac{2\pi pc}{eL}$$

$$\omega_{e min} = \sqrt{3} \frac{\pi}{L} \quad ; \quad j_{emin} = \frac{3\pi}{2L^2} \frac{pc^2}{e} \quad ; \quad \beta_{in} = \frac{L}{2\pi} \quad (5.33)$$

The value of j_{emin} is given here for the exact neutralization of electric field of the electron beam ($\mathcal{K} = 1$, $\mathcal{F} = -\beta^2$; see (5.7,8)).

V.4 Parameter choice. Accumulation Rates.

Let us take the antiproton energy in the cooler to be 400 MeV and the length of each of the two cooling sections to be $L = 100\text{m}$. The results, which were obtained above allow us to calculate the values of the other parameters. The results of such calculations are presented in Table I, where cases to be discussed below are also presented.

Let us suppose, also, that the proton beam in U-70 before extraction is bunched in short bunches, each of whose length is 1 m with 1.6×10^{12} p/bunch. For \bar{p} -production 4 bunches of 30, in total, are used.

CASE A: This is the case giving maximum accumulation rate, having cooling straight sections with unit transfer matrix. For this case the solenoid field and electron current density are given by expressions (5.33) so, in order to have

$$M_{\text{cool}} = -I \quad (5.34)$$

one takes the cooling time equal to the cycle duration,

$$\tau_{\text{cool}} = \tau_{\text{cycle}} = 7 \text{ sec} \quad (5.35)$$

from (4.4,5) one obtains the maximum values for θ_0 , θ , θ_{\perp} which are acceptable for given j_e . These angle parameters give the \bar{p} emittance value ε :

$$\varepsilon = \beta \theta_1^2 = \frac{L}{3\pi} \theta_0^2 \quad (5.36)$$

The \bar{p} -beam emittance injected into the decelerator is p_{cool}/pt times smaller than ε , and defines the meaning of the efficiency F (see Fig. 3). The \bar{p} momentum spread is given by the value of θ (4.5). From (3.4) the accumulation rate can be calculated.

The electron beam size is taken equal to the \bar{p} -beam size in the cooling section (see (5.27)):

$$a_e = \frac{L \theta_0}{\pi \sqrt{6}} \quad (5.37)$$

The realization of Case A possess very complicated technical problems. It is possible to relax these requirements if the accumulation

rate is only a little diminished. The simplest way is represented by:

CASE B: Decreased accumulation rate but still unit transfer matrix for cooling section.

Let us leave the values of the solenoid field and current density the same as in the case A, i.e.

$$M_{\text{cool}} = -I$$

but take ϵ equal to 360 mm.mrad instead of the maximum value 940 mm.mrad. Then from (5.35) one obtains a value for θ_0 ; from (4.45) θ , θ ; from (5.37) A_e and so forth. In case B the cooling time is much shorter than the cycle duration. This reserve performance results from a desire to retain the unit matrix cooling section condition; it can be used in:

CASE C: Diminished accumulation rate with non unit matrix straight sections.

If one chooses, as before, \bar{p} beam emittance in the cooler equal to 360 mm.mrad, one can calculate all parameters for the condition (5.35). Then, to fix j_e and θ_0 it is necessary to solve the system of equations which follow from (4.4) and (5.25):

$$j_e = \frac{\beta^4 r^5}{180\pi} \frac{mc^3}{e} \frac{\theta_0^3}{c r_p \eta \tau_e} \quad (5.38)$$

$$\epsilon = \beta \theta_1^2 = \frac{2}{3} \frac{\theta_0^2}{\sqrt{\omega_H^2/4 + \omega_c^2}} \quad \omega_e^2 = \frac{2\pi e j_e}{\beta \gamma M c^3}$$

The equation following from (5.38) has the form,

$$\epsilon = \beta \theta \frac{\theta_0^4}{\epsilon^2} = \frac{1}{40} \frac{\beta^3 r^4}{c r_p \eta \tau_e} \frac{m}{M} \theta_0^3 + \frac{9}{16} \omega_H^2 \quad (5.39)$$

Its solution for θ_0 gives the parameter values which are shown in Table I, case C. The loss in accumulation rate (4.5 times compared to Case A.) is "compensated" by the essential simplification of the electron cooling system. However, in this case the transfer matrix is not unity, so lattice compensation is necessary.

The cases A, B and C compass the practically possible range in the parameter "game".

Calculations for these cases are made supposing the absence of coupling between ring halves. It is useful to retain the solenoid field value as a free parameter. For this reason two additional solenoids can be placed at both ends of the straight section whose fields can attain:

$$\int H_{||} ds \sim 50 \text{ kG m}$$

for each solenoid. These solenoids could be superconducting with relatively small size.

The electron beam in the cooler is very high powered - about 100 MW for even the easiest case C. Incorporation of electron energy recovery^{/8/} will decrease the consumed power by a factor of 50-100.

The electron cooling system solenoid is a major component of the construction. Its approximate parameters are: internal dia. 20 cm; external dia. 30 cm; copper weight for the windings, 73 ton; power supply, 1.6 MW for a 2 kG field.

Table 1
Cooler-Accumulator Parameters

Antiproton energy	400 MeV			
Antiproton momentum	954 MeV/c			
Electron energy	218 MeV			
Circumference	250 m			
Average radius	39.8 m			
Cooling section lengths	2 x 100 m			
Orbit ratio, occupied by electron beam	0.8			
Solenoid magnetic field	2 kG			
		<u>CASE A</u>	<u>CASE B</u>	<u>CASE C</u>
Antiproton beam parameters in cooler:				
parameter θ_0 , mrad	9.4	5.8	4.4	
angle spread θ_{\perp} , mrad	7.7	4.8	3.6	
momentum spread, 10^{-3}	7.7	4.7	3.6	
emittance, mm.mrad	940	360	360	
Antiproton beam parameters after target:				
momentum spread, %	± 8.4	± 3.2	± 3.2	
emittance, mm.mrad	160	60	60	
Electron cooling system parameters:				
electron current density A/cm ²	1.5	1.5	0.15	
electron density, 10^8 cm ⁻³	4.4	4.4	0.44	
beta function in cooling system, m	15.9	15.9	27.8	
electron beam radius	12	7.5	10	
electron beam current, A	680	265	47	
reactive power of electron beam, MW	148	58	10	
Antiproton number per cycle, 10^8	17	3.2	2.5	
Accumulation rate, 10^7 sec ⁻¹	24	4.7	3.6	

V.5 Cooler Lattice

The cooler lattice includes two solenoids with electron beam and two half rings of 25 m length each. We consider the case of transfer matrix $M = -I$.

The characteristics of this lattice stem from the necessity to have, in the cooling section

$$\beta_x = \beta_z = \omega_c^{-1} \quad \beta'_x = \beta'_z = 4 = 0$$

(see (5.25)). These conditions can be realized with a lattice of the FODO type, as is shown in Ref. 9. These results are represented in Fig. 8. The betatron frequencies for the ring halves and their transition energy are equal to

$$\nu_x = 2.112 \quad \nu_z = 1.585 \quad \gamma_t = 2.21$$

The chromaticity is

$$\frac{d\nu_x}{d(\Delta p/p)} = -5.51 \quad \frac{d\nu_z}{d(\Delta p/p)} = -1.75$$

If the initial momentum spread of the \bar{p} -beam is equal to $\pm 4 \times 10^{-3}$, we have

$$\Delta\nu_x = 0.022 \quad \Delta\nu_z = 0.007$$

even without chromaticity correction. The maximum of β_z in the magnets is equal to 9 m. This corresponds, for an emittance of 360 mm.mrad, to a vertical beam size of ± 5.6 cm. The maximum

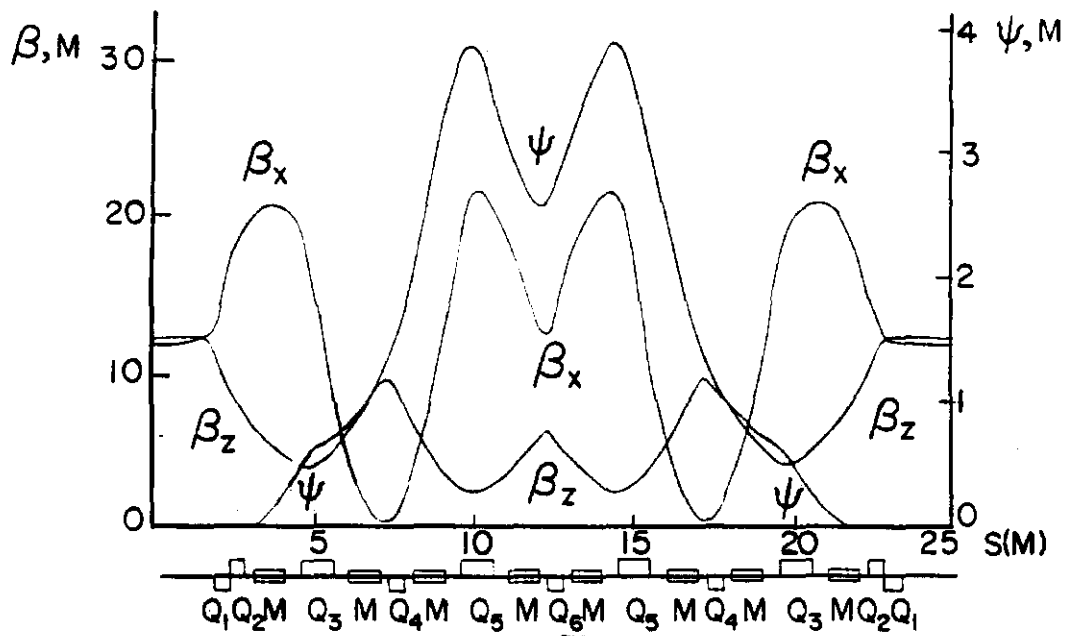


Fig. 8 Betatron and dispersion functions for half rings on cooler. Here $Q_1 - Q_6$ are quadrupoles, M - bending magnets.

radial size of the beam is ± 3.7 cm. Therefore, the apertures can be,

$$A_z = \pm 6 \text{ cm}, \quad A_x = \pm 10 \text{ cm}$$

Parameters of this lattice are given in Table 2.

Table 2
The Cooler Lattice Parameters

<u>See (Fig. 8)</u>	<u>Name</u>	<u>B, kG</u>	<u>∇B, kG/cm</u>	<u>Length</u>
Q ₁	Quadrupole lens	--	-0.2	0.5
Q ₂	" "	--	0.1	0.5
Q ₃	" "	--	0.116	1
Q ₄	" "	--	-0.29	0.5
Q ₅	" "	--	0.14	1
Q ₆	" "	--	-0.33	0.5
M	Dipole	12.5	0	1

V.6 Antiproton Beam Lifetime in the Cooler.

Antiproton lifetime in the storage ring with electron cooling is limited by Coulomb single scattering greater than the aperture angle and by nuclear absorption of antiprotons by ions, which are trapped in the electron beam for space charge neutralization.

The cross-section for single scattering, for angles larger than θ_{\max} , is equal to

$$\sigma = \frac{4\pi r_p^2}{\beta^4 \gamma^2 \theta_{\max}^2} \quad (5.40)$$

The dependence of these cross-sections versus \bar{p} -momentum is shown

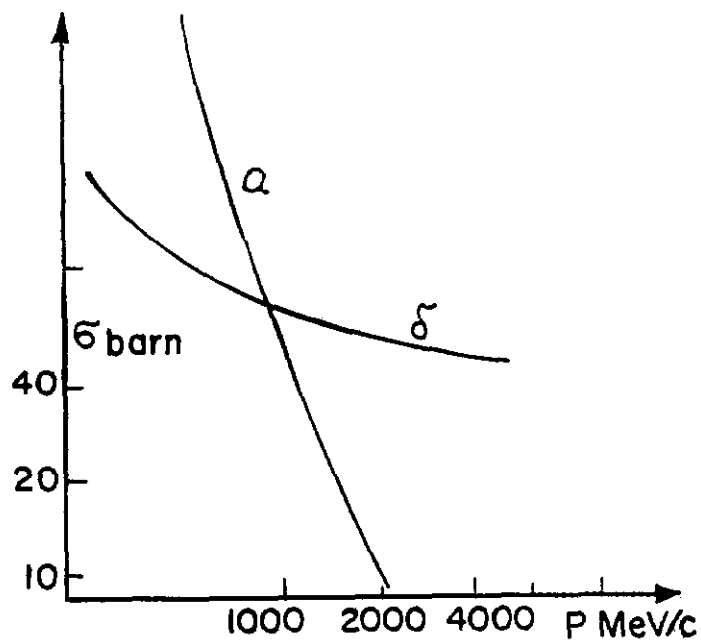


Fig. 9 The dependence of single scattering and nuclear absorption cross sections on p momentum.

a. Single scattering, for $\theta_{\max} = 3$ mrad.

b. Nuclear absorption

in Fig. 9 for H ions. Both cross sections are approximately equal, if $pc = 1 \text{ GeV}$, and the cross section value is equal to 13 mbarn. In this case, and for ion density in the electron beam $n_i = 4 \times 10^8 \text{ cm}^{-3}$ the antiproton lifetime is equal to

$$\tau = (\gamma n v \sigma)^{-1} = 1.1 \cdot 10^6 \text{ sec} \approx 13 \text{ hr.}$$

Obviously, the residual gas density must be much lower than the ion density in order not to contribute additionally to the \bar{p} life time:

$$p < \frac{10^{-8}}{Z^2} \text{ Torr}$$

V.7 Emittance of Accumulated Antiprotons. Luminosity and its Life time.

The transverse emittance of an intense antiproton bunch depends on the interaction of antiprotons within the beam. Experiments which have been done at NAP-M show that the space charge effects increase transverse dimensions of the beam when the tune shift, $\Delta\nu$, reaches 0.15. Future increases of beam current will lead to proportional increases of the beam cross section. Assuming $\Delta\nu_{\bar{p}\bar{p}}$ constant one can estimate the transverse emittance of the beam after accumulating N particles in a bunch of length l . The betatron tune shift, $\Delta\nu_c$ in the accumulator is

$$\Delta\nu_c = \frac{r_p}{2\pi \beta^2 \gamma^3} \frac{N_{\bar{p}}}{l} \frac{\beta_0 R_0}{a^2} \quad (5.41)$$

where β_0 , R_0 are the betatron function and average radius of the ring, πa^2 is the cross section of the beam. Eq. (5.41) yields the minimum emittance of a cooled beam

$$\varepsilon_{cool} = \frac{a_0^-}{\beta_0} = \frac{r_p N_{\bar{p}} R_0}{2\pi \beta^2 \gamma^3 L \Delta \gamma_c} \quad (5.42)$$

If we take $\ell = 10$ m, $\Delta \gamma_c = 0.15$, $N_{\bar{p}} = 1 \cdot 10^{11}$, Eq. (5.42) gives $\varepsilon_{cool} = 0.5$ mm mrad. Acceleration of the beam to experimental energy, E_{exp} , leads to adiabatic decrease of the beam beam emittance up to

$$\varepsilon_{min} = \begin{cases} 1.25 \cdot 10^{-3} \text{ mm mrad for } E_{exp} = 400 \text{ GeV} \\ 1.6 \cdot 10^{-4} \text{ mm mrad for } E_{exp} = 3 \text{ TeV} \end{cases} \quad (5.43)$$

provided dilution of emittance during acceleration is negligible.

It is well known that the luminosity of colliding beams depends on the beam-beam tune shift

$$\Delta \nu_{p\bar{p}} = \frac{N_p r_p}{2\pi \varepsilon_p \gamma_{exp}} \quad (5.44)$$

We hope to reach $\Delta \nu_{p\bar{p}}$ up to 10^{-2} by increasing the cross section of the proton beam with constant density thus decreasing nonlinearities of the force acting on the antiproton beam. Experiments which have been done at VEPP-2M confirm this assumption.

Equation (5.44) yields for, $N_p = N_{\bar{p}} = 10^{11}$, and $\varepsilon_p = \varepsilon_{\bar{p}}$

$$\varepsilon_p = \begin{cases} 6 \cdot 10^{-3} \text{ mm mrad for } E_{exp} = 400 \text{ GeV} \\ 8 \cdot 10^{-4} \text{ mm mrad for } E_{exp} = 3 \text{ TeV} \end{cases} \quad (5.45)$$

Estimates (5.43) and (5.45) show that the luminosity is determined by the emittance eq. (5.45). So we may write

$$\mathcal{L} = f_0 \frac{N_p N_{\bar{p}}}{\pi E_p \beta_{exp}} = 2f_0 \frac{N_p \Delta V_{p\bar{p}}}{r_p \beta_{exp}} \gamma_{exp} \quad (5.46)$$

If we use here $f_0 = 1.5 \cdot 10^4 \text{ sec}^{-1}$, $N_p = N_{\bar{p}} = 10^{11}$, $\beta_{exp} = 1 \text{ m}$, the luminosity will be

$$\mathcal{L} = \begin{cases} 8 \cdot 10^{29} \text{ cm}^{-2} \text{ sec}^{-1} & \text{for } E_{exp} = 400 \text{ GeV} \\ 6 \cdot 10^{30} \text{ cm}^{-2} \text{ sec}^{-1} & \text{for } E_{exp} = 3 \text{ TeV} \end{cases} \quad (5.47)$$

The luminosity life time is mainly determined by intrabeam scattering in the bunches. In the smooth approximation and with strong coupling in betatron motion we can write

$$\frac{d\epsilon}{dt} \approx \frac{\epsilon}{\tau_{is}}, \quad \tau_{is} = \frac{\gamma^3 l (2\epsilon)^{5/2}}{c r_p^2 N R_0^{1/2}} \quad (5.48)$$

For the case of UNK⁽¹¹⁾ $R_0 = 3070 \text{ m}$, $\nu = 40.75$, and emittance given by (5.45), the luminosity life time will be

$$\tau_{is} = \begin{cases} 5 \cdot 10^5 \text{ sec} & \text{for } E_{exp} = 400 \text{ GeV} \\ 7 \cdot 10^5 \text{ sec} & \text{for } E_{exp} = 3 \text{ TeV} \end{cases} \quad (5.49)$$

This is approximately 10 times less than the beam life time due to the scattering with residual gas equivalent to a hydrogen pressure of 10^{-8} torr.

V.8 Electron Cooling for Protons

Achieving high luminosity requires both antiproton and proton beams to have minimal emittance and, correspondingly, high densities. It may happen that the existing RF system of the U-70 synchrotron and its booster upgrading project will not be able to provide the necessary quality proton beam. Then it would be useful to utilize the antiproton source rings for producing high density proton beams. For this purpose protons can be injected via a special linear accelerator (with proton energy ~ 10 MeV) into the synchrotron decelerator and be accelerated to cooling energy (400 MeV). Then, after electron cooling, the protons will be accelerated in the decelerator synchrotron, U-70, and the first UNK ring. Both beams meet in the second ring for acceleration and cooling.

If injection energy for the decelerator is equal to 10 MeV, the betatron tune shift due to proton beam space charge will be about 5×10^{-3} (transverse beam size is ± 3 cm, with first harmonic RF). The bending magnet fields for such energy is 350 G. For proton acceleration it is necessary to create an additional RF system on the first harmonic with a tuning range of $175 \div 855$ kHz.

VI. DECELERATION SYNCHROTRON

VI.1 Lattice, Injection, and Extraction

The deceleration synchrotron for case B (Table I) is described below. For case A, aperture requirements are $\sim \times 1.6$ larger.

The transition energy is chosen to be $\gamma_{\tau} = 7$, (energy 5.6 GeV) in order to facilitate RF rotation. The betatron tunes should be roughly the same: $\beta_x \sim \beta_y \sim \gamma_{\tau} \sim 7$. For a 90° phase advance per cell, the number of cells in the lattice should be $N \sim 4 \times 7 = 28$. With a deceleration circumference of 200 m, the cell length is $2 \pi R_0/N = 7.1$ m. Each cell consists of a FODO focusing structure with separated function. The magnetic field at production energy is 13.9 kG in bends, 1.8 kG/cm gradient in quadrupoles. Figure 10 shows the arrangement of elements and the betatron and dispersion functions for one cell. For this structure

$$\nu_x = 7.89, \quad \nu_y = 7.56, \quad \gamma_t = 7.04$$

The decelerator acceptance is chosen to equal the decelerated \bar{p} beam emittance: $\epsilon = 360$ mm.mrad, $\Delta p/p = 4 \times 10^{-3}$. With $\beta_{\max} = 12$ m (Figure 10) the betatron size is $a_{\bar{p}} = 6.6$ cm. With dispersion $\psi_{\max} = 1$ m, the horizontal width due to momentum spread is $\Delta r_{\psi} = 0.4$ cm. The radial aperture requirement is thus $A > a + \Delta r_{\psi} = \pm 7$ cm. After injection and before RF rotation the beam sizes are $a = 2.7$ cm, $\Delta r_{\psi} = 3$ cm.

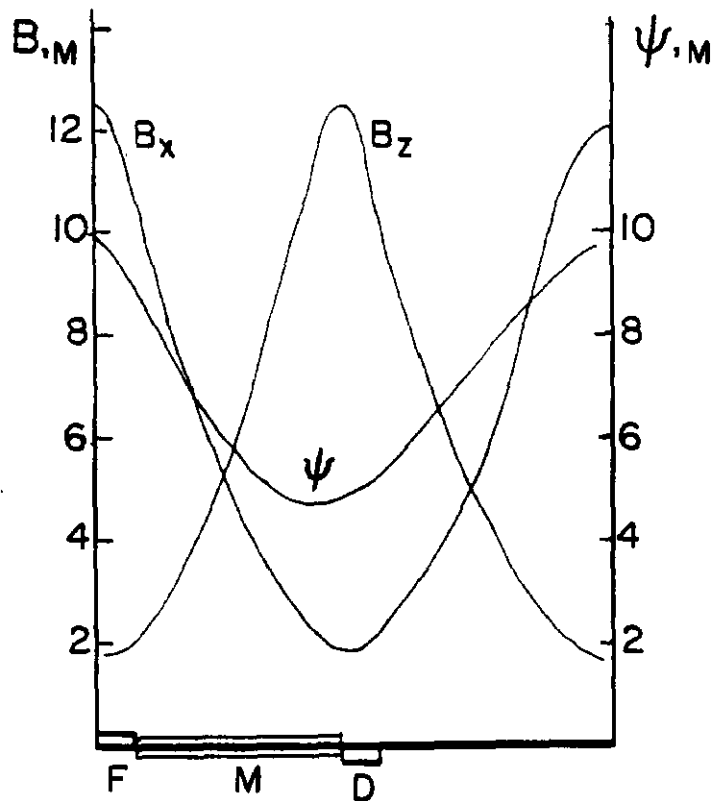


Fig. 10 Betatron and dispersion functions for the decelerator, with periodicity elements. FMD: F - focusing quad., D - defocusing quad. (lengths = 0.5 m), M - bending magnets.

Table 3

Decelerator synchrotron parameters

Circumference	200 m		
Transition energy	5.6 GeV ($\gamma_t = 7.04$)		
Injection energy	4.7 GeV ($\gamma_i = 6$)		
Injection momentum	5.5 GeV/c		
Revolution frequency	1.48 MHz		
Initial momentum spread of \bar{p} beam	$\pm 3.2 \cdot 10^{-2}$		
Bunch length after injection	1 m		
Bunch number	4		
RF - system	RF rotation		Deceleration
frequency, MHz	17.748	35.496	5.916
harmonic number	12	24	4
voltage amplitude, KV	1000	150	40 → 70
RF rotation duration			140 μ sec

Lattice

Periodicity number	4 x 7 = 28		
Periodicity element length	7.143 m		
Bending field	13.9 kG		
Magnets radial aperture	± 7.5 cm		
Lens field gradient	1.8 kG/cm		
Betatron numbers	$\nu_x = 7.559, \nu_z = 7.888$		
Acceptance	360 mm.mrad		

Decelerator parameters are presented in Table 3.

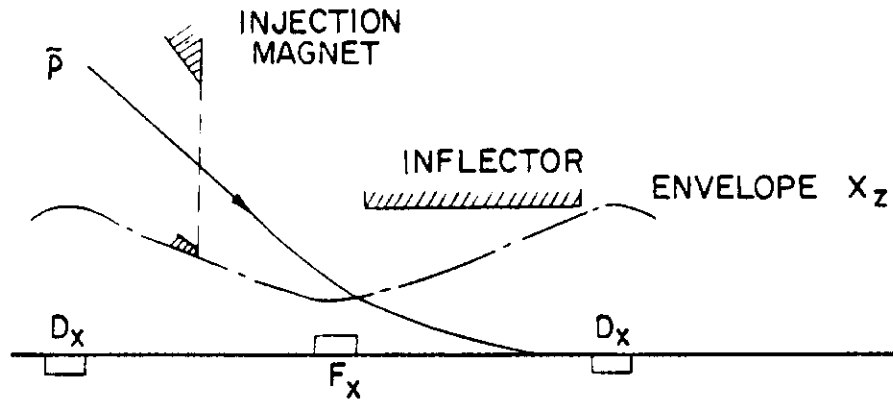


Fig. 11 Arrangement of injection into the synchrotron decelerator.

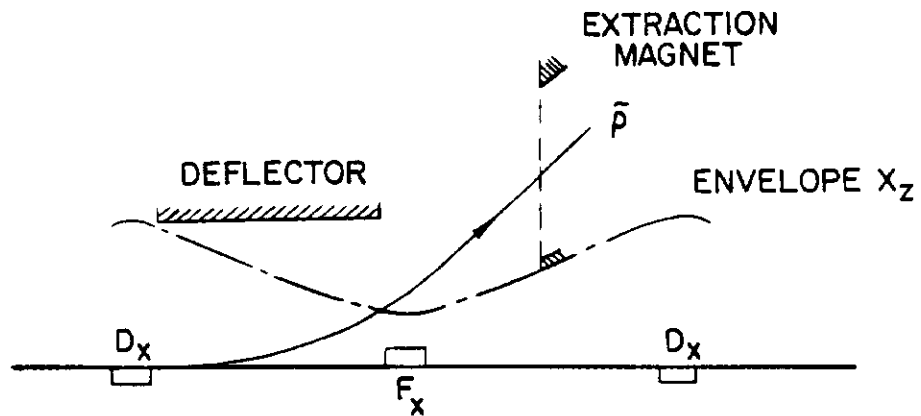


Fig. 12 Arrangement of extraction from the synchrotron decelerator.

Injection and extraction are accommodated in the vertical plane (Figures 11,12). The two systems each occupy two adjacent straight sections. The injection septum occupies the first half of one straight section. The deflector occupies all of the next straight section. The septum and deflector magnets are outside the vacuum envelope. The maximum distance of the injected (extracted) beam is small at the location of the focusing lens. The maximum excursion is ~ 3 times larger at the location of the defocusing lens, where beam size however is minimum. Thus all quadrupoles have roughly equal apertures, and can be made alike.

The deflectors for injection and extraction are full aperture ferrite kickers. The deflectors can be removed from the aperture after injection, and inserted into the aperture only during injection. In this way the inflector current can be reduced by a factor 3. The general parameters of the injection system are given in Table 4.

VI.2 RF System

The RF system for the decelerator must be able to 1) create RF rotation of \bar{p} bunches in order to reduce momentum spread; 2) decelerate \bar{p} beam to cooling energy. The method of RF rotation to reduce momentum spread has been described in Ref. 4. In order to reduce to a minimum the required RF voltage, the decelerator lattice is designed so that the energy of the injected \bar{p} 's is close to transition energy.

Table 4

The parameters of injection-ejection system

Injection

Antiproton momentum	5.5 GeV/c
Beam emittance	300 mm.mrad
Momentum spread	$\pm 3.2\%$
Injection magnet aperture	7.5 x 4 cm.cm.
Inflector aperture	14.5 x 13.5 cm.cm.
Injection angle	-1.7 mrad
Inflector current	7 kA
Inflector current disappearing time	150 msec
Inflector current pulse duration	700 msec

Ejection

Antiproton momentum	0.95 GeV/c
Beam emittance	360 mm.mrad
Momentum spread	$\pm 0.4\%$
Ejection magnet aperture	9.5 x 9.5 cm.cm.
Deflector aperture	14.5 x 13.5 cm.cm.
Beam displacement near injection magnet wall	9.5 cm.
Ejection angle	-19 mrad
Deflector current	2.5 kA
Deflector current pulse duration	700 msec
Front duration of deflector pulse	50 msec

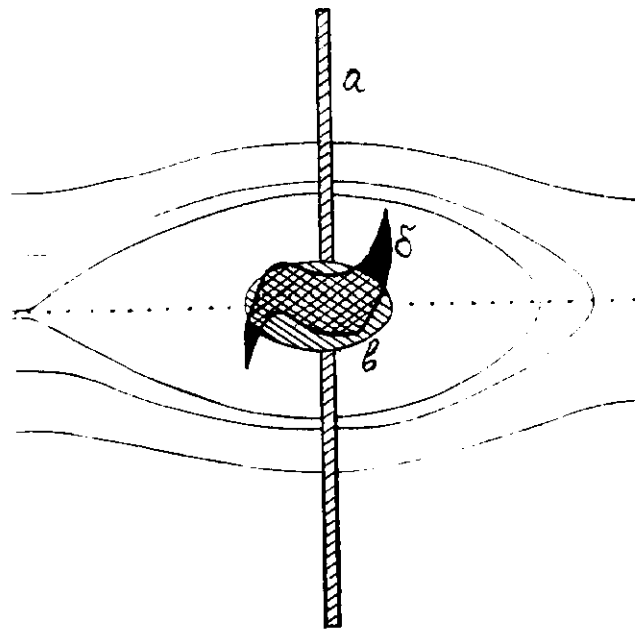


Fig. 13 Antiproton longitudinal phase space capture in decelerator, a, at injection, before rotation; b, after rotation; c, area available for cooling after deceleration; d, 4th harmonic separatrix.

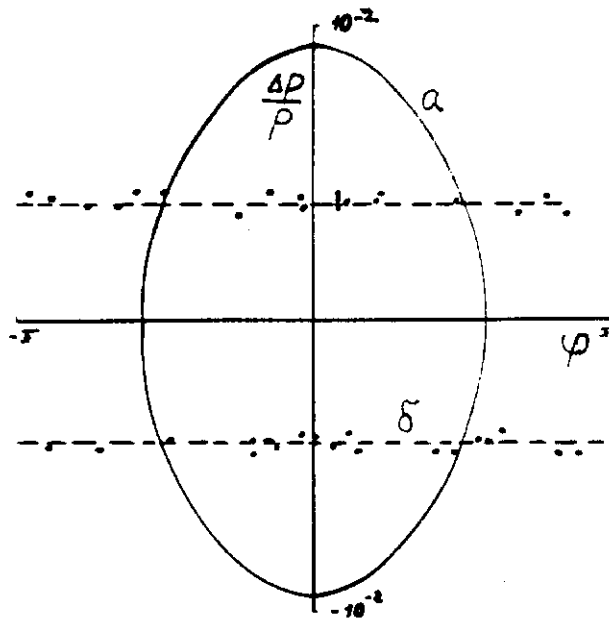


Fig. 14 Adiabatic debunching of \bar{p} beam
 a - \bar{p} longitudinal area after deceleration
 b - after slow (~ 10 msec) switch off of RF.

Phase rotation and deceleration are described in Figures 13, 14, and proceed as follows:

1) The short injected bunches of \bar{p} 's are rotated in longitudinal phase by an angle $\pi/2$. Two RF systems are used for this purpose, with parameters given in Table 3. The \bar{p} momentum spread is reduced so that 85% of the stored beam intensity will be captured in a separatrix having the following parameters:

$$\begin{aligned} \frac{\Delta p}{p}_{\max} &= 4.5 \times 10^{-3} \\ \phi_{\max} &= 0.72 \\ s &= \pi \phi_{\max} \frac{\Delta p}{p} = 10^{-2} \quad (\pi \Delta p \times L_B = 5.8 \text{ eV sec}) \end{aligned}$$

The duration of the RF rotation is 140 μ sec.

2) For deceleration the \bar{p} 's are captured on harmonic 4. During deceleration the RF voltage is gradually increased (40 \rightarrow 70 kV) to just contain the beam. The deceleration rate is 6 GeV/sec. After deceleration the beam has the following parameters:

$$\begin{aligned} \frac{\Delta p}{p}_{\max} &= 9.5 \times 10^{-3} \\ \phi_{\max} &= 1.86 \\ s &= 5.8 \times 10^{-2} \quad (5.8 \text{ eV sec}) \end{aligned}$$

3) After deceleration the beam is debunched in a time 10 msec. The momentum spread of the DC beam is $\frac{\Delta p}{p}_{\max} = 4 \times 10^{-3}$, $\phi_{\max} = \pi$.

4) The described scheme is illustrated by Fig. 13, 14. The RF system parameters have the following values:

ferrite cross section	$4 \cdot 10^3 \text{ cm}^2$,
ferrite circles radii	10 x 20 cm,
cavity (resonator) length	400 cm
ferrite weight	1.8 t

The energy, captured in ferrite, is equal to 34 joules. If power loss efficiency is $\text{tg } \delta = 0.02$, the necessary power is equal to 11 MW for 120 msec and frequency 17.7 M.

VI.3 Decelerator Synchrotron Magnet

The magnet cross section is shown in Fig. 15. Magnet parameters are given in Table 5.

Table 5

The same technical parameters of
magnet for decelerator-synchrotron

Magnet length	3 m
Maximum magnetic field	14 kG
Whole iron weight	100 t
Whole copper weight	60 t
Weight of each magnet	5.2 t
Maximum current density	370 A/cm^2
Pulse power losses in each magnet	1.8 MW
Average power losses in each magnet	0.26 MW
Average power losses in all magnets	7.3 MW
Maximum current	170 KA

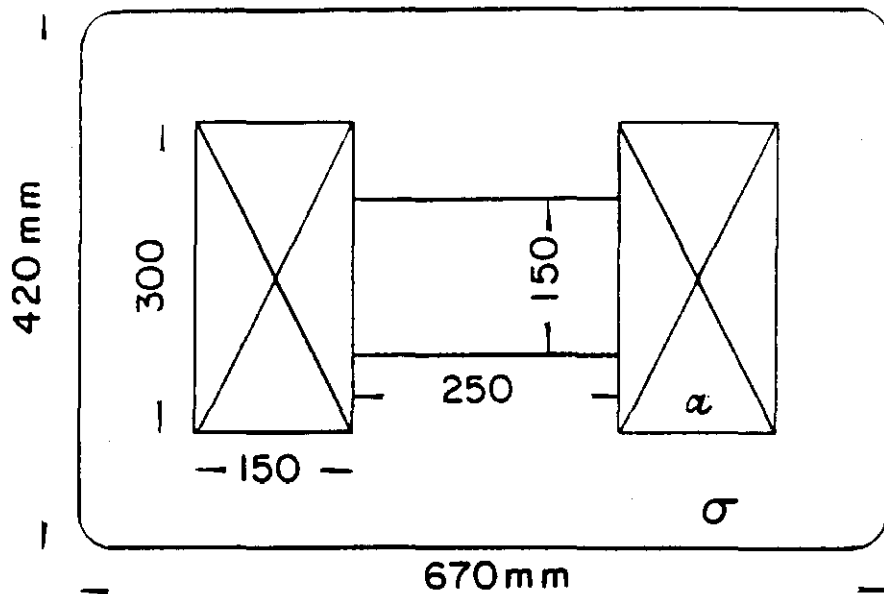


Fig. 15 Magnet cross section for the decelerator synchrotron.
 a - coils , b - flux return yolk

VII. POSSIBILITIES FOR FUTURE IMPROVEMENT OF THE ANTIPROTON SOURCE

Several possibilities for improving the \bar{p} source are discussed below. It should be noted that the various improvements are not independent; in particular the debuncher ring would be superfluous if stochastic cooling of intense beams could be made practical.

VII. 1 PROTON DELAY CHANNELS

The present \bar{p} source design uses only 4 of the 30 proton bunches from the U-70 synchrotron. But the \bar{p} collection rate is proportional (see 3.4) to line density of the extracted proton beam, and not on bunch number. So if more bunches were targeted, the line density would remain the same and the \bar{p} collection rate would not be increased.

On the other hand, the \bar{p} transverse emittance density depends only very weakly on the proton beam emittance, since the \bar{p} acceptance is much larger than the proton emittance. If several proton bunches could be targeted at the same time, converging to a common target spot, the \bar{p} phase space density would be increased proportionately.

The required system would consist of several ($N \leq 7$) channels, each differing in transit time by one bunch spacing. N consecutive bunches would be extracted from U-70, and enter a special deflector. The deflector would be driven by a staircase waveform $\alpha = (N-n)$, so as to direct each bunch into its appropriate channel. After appropriate path lengths $s = s_0 n$, the bunches would each be focused by N lithium lenses, displaced transversely and having a common focus at the target. The lens displacement is limited by the beam convergence angle, which must be smaller than the \bar{p}

collection angle.

Consider the case of 7 proton beams, each having an emittance $2 \times 10^{-6} \text{m}$, focused to a common spot with radius .45 mm. If the distance between beam axes at the lens is taken to be twice the beam diameter, the equivalent emittance contribution of each beam is diluted a factor of 5. The \bar{p} collection efficiency in an acceptance of $70 \times 10^{-6} \text{m}$ will be 97% of that for one beam in the same spot size.

Twenty-eight bunches of protons are transformed into 4 bunches at the target. The 4 \bar{p} bunches must be injected into the Decelerator using an inflector with 4 current pulses. The length of each bunch is ≤ 250 nsec, separated by 1170 nsec. The basic design of the required power supply has been developed at INP. Perhaps the simplest realization of the inflector requirements would be to locate 4 independent deflectors in one straight section of the Decelerator. In this case the rise time requirement is relaxed, and the inflector can be driven as usual by a unipolar sinusoid pulse with ~ 250 nsec duration.

The delay channels must have path lengths which differ by multiples of $L_B = 50 \text{m}$. Such an arrangement is simple in principle, but involves a bulky construction. One arrangement is shown in Figure 16. The total length of the transport line is 2 km. The bunches are separated at extraction into 6 bending sections with deflection angle 12.7° , 5° , 3.8° , 3.1° , 2.7° , and 2.3° . Over the major path length of the channels, the beams are bent to produce appropriate

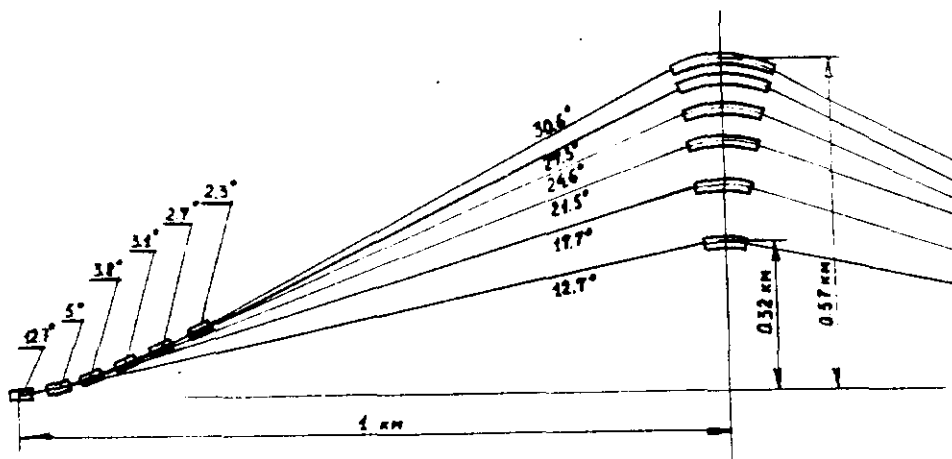


Fig. 16 The delay channels

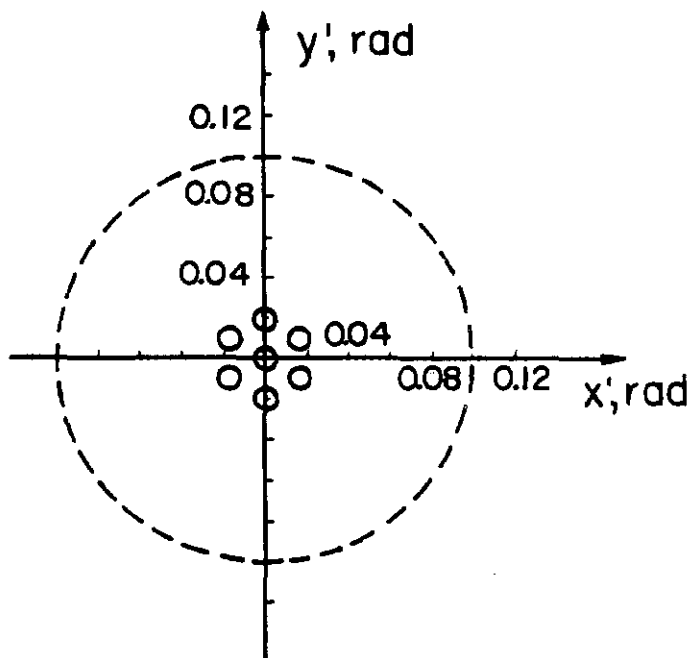


Fig. 17 Scheme of proton bunch focusing at the target center plane. Dotted curve gives angular acceptance.

path lengths. The total bending in all channels is 270° . At the end of each channel is a 3-dimensional deflection system to steer each beam to its lithium lens. The septum magnets used to recombine the beams have a total bending angle of 27.6° , the same as at the channel entrance. Thus, the channels require a total bend of 330° , and a total transport length of 13 km.

The transport lines would be constructed in standard concrete drainage pipe, ~ 1 m diameter, as at Fermilab. A total of ~ 200 quadrupoles provide a regular FODO focusing structure along the transport lines. The magnetic elements would probably have single turn conductors and be pulsed only during \bar{p} production. The total stored magnetic energy is estimated to be ~ 5 MJ. The average power is estimated to be ~ 1 MW.

Other schemes of delay channels have been considered, for example with 600 m transport, total bending 850° with bending radius 150 m, or total bending 580° with bending radius 50 m.

The delay channel arrangement should increase \bar{p} collection by a factor 7: $\dot{N}_{\bar{p}} = 3.5 \times 10^8 \text{ sec}^{-1}$. The channels can be added as a later improvement, with $\dot{N}_{\bar{p}}$ proportional to the number of channels.

VII.2. The buncher ring

Improvements in the U70 synchrotron are expected to reduce the proton momentum spread to $\leq 2 \times 10^{-4}$ (similar to the Fermilab main ring). The bunch length can then be reduced to such an extent that all four bunches can be combined head-to-tail into a single bunch having the length of one present bunch.

This transformation could be performed in a debuncher ring with a circumference of $\sim \frac{1}{4}$ that of the U70 synchrotron. Since the magnetic bending radius is then 4 times larger, the bending field is then $\sim 4T$, and UNK magnets can be used.

In a dispersion-free region of the debuncher ring is located a tungsten target with thickness $\Delta = \lambda_{\text{nuc1}}/3 (n-1)$, λ_{nuc1} is the nuclear absorption length, and n is the number of turns required. If protons are injected on the outermost region of the momentum aperture, they will lose an amount of energy $\Delta E = 200/\text{MeV}/3(n-1)$ per target crossing. A septum magnet is located in a region of maximum dispersion. The beam displacement there will be

$$\Delta r = \psi_s \left(\frac{\Delta p}{p} \right)_t$$

The beam will leave the septum if $\left(\frac{\Delta p}{p} \right)_t \psi_m \geq 2 \sqrt{\psi_s^2 \left(\frac{\Delta p}{p} \right)_p^2 + \epsilon_p \beta_s}$ where ψ_s is the dispersion at the septum, and $\left(\frac{\Delta p}{p} \right)_p$, ϵ_p , β_s are the momentum spread and emittance of the proton beam, β_s is the beta function at the septum. For $\left(\frac{\Delta p}{p} \right)_p = \pm 1 \times 10^{-4}$, $\left(\frac{\Delta p}{p} \right)_t = 2.5 \times 10^{-4}$, $\beta_s = 10 \text{ m}$ a dispersion of $\psi_s \geq 50 \text{ m}$ is required. The target crossing will not excite betatron oscillations due to energy loss if ψ_t and ψ'_t are both zero at the target. The rms scattering angles $\langle \theta^2 \rangle$ will not dilute the emittance if $\beta_m \ll \epsilon_p / \langle \theta^2 \rangle$. After the first bunch has made 4 revolutions all 28 bunches will be captured in the ring. The bunches will be separated in the momentum, but

will overlap where $\psi = 0$. The first bunch will cross the target 3 times, and will be attenuated by $\sim 30\%$ due to nuclear absorption. The average attenuation will be $\sim 15\%$. After all 4 bunches are in the buncher ring, the entire beam will be extracted in a single turn and targeted to produce antiprotons. Extraction is performed at a zero-dispersion point, so as to minimize chromatic aberrations in the extracted beam. Exact coincidence of the 4 bunches will be insured if the ratio of U-70 and bunches radii is 4, and momentum compaction is near zero.

The extracted proton super bunches are transported through 7 delay channels as described above and focussed to a common target. The result is a single \bar{p} bunch with 28 times the original phase space density.

If the improvements to U-70 do not succeed in reducing the present momentum spread of $\sim 10^{-3}$, the bunches could only be used after first reducing the momentum spread using a wedge. The proton beam would be passed through a wedge-shaped target. By locating the target in a region of maximum dispersion, the correlation of momentum and energy loss can reduce the momentum spread of the beam (at the cost of increasing the betatron amplitudes). The ionization loss will be dependent on the vertical coordinates Z of each particle:

$$-\delta\varepsilon = \alpha \left(Z_p + \psi_v \frac{\Delta p}{p} \right)$$

The coefficient α is proportional to wedge angle and depends on target material characteristics. The average energy loss is

$$\langle -\delta\varepsilon \rangle = \alpha \left(\langle Z_p \rangle + \psi_v \left\langle \frac{\Delta p}{p} \right\rangle \right) = \alpha \left(\sqrt{\Sigma_{3t}} + \psi_v \left\langle \frac{\Delta p}{p} \right\rangle \right)$$

The final momentum spread is

$$\left\langle \frac{\Delta p}{p} \right\rangle_f^2 = (1 - \alpha \psi_V)^2 \left\langle \frac{\Delta p}{p} \right\rangle_i^2 + \left(\frac{\alpha \sqrt{\epsilon \beta_t}}{p} \right)^2$$

Choosing $\psi_V = \alpha^{-1}$, we obtain $\left\langle \frac{\Delta p}{p} \right\rangle_f = \frac{\sqrt{\epsilon \beta_t}}{\psi_V p}$. The beam emittance dilution from multiple scattering is also proportional to β_t . For both reasons β_t must be chosen to be 1 m or less.

The gain in \bar{p} phase space density can be realized in full if the one superbunch of antiprotons can be debunched in the Decelerator in the manner described in Section VI.2. If the single superbunch could only be debunched to fill 1/4 of the Decelerator circumference (as for the design of Section VI.2), the remaining 3/4 of the circumference could be filled with antiprotons from neighboring regions of the \bar{p} energy spectrum. A system of lithium lenses could be located at a point following the target with large dispersion, so that various momentum components will be separated in the lens focal plane. A spectrometer magnet can then be used to further separate the momentum components into n individual beams. Each beam would then be refocussed through another lithium lens, and passed through an appropriate delay channel. It would be necessary to reaccelerate each beam to the Decelerator momentum p_0 , requiring acceleration $\Delta p, 2\Delta p, \dots, (n-1)\Delta p$ in special synchrotrons. The reacceleration time would be ~ 1 msec. The successive beams would then be injected into the Decelerator where RF rotation and debunching would proceed as before. The scheme for this process is shown in Figure 18.

The design of the special synchrotrons would appear to be much simpler and cheaper than that of the decelerator, mainly because the energy change required is $\sim 5-15\%$, and the required acceptance is ~ 5 times smaller. The injection and extraction systems are much simpler because of the small acceptance. The RF system must be capable of capturing a momentum spread

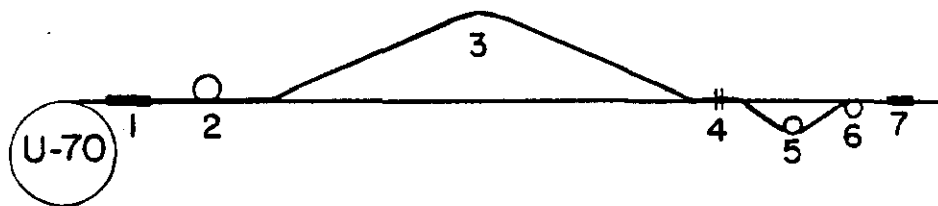


Fig. 18 Plan for improved antiproton source.

1. Monochromating target; 2. Buncher;
3. Delay channels; 4. Target station
5. Monochromating synchrotron;
6. Decelerator synchrotron;
7. Accumulator

$\sim 3\%$, requiring an amplitude $\sim 1-2$ MV.

VII.3 Multitarget designs

The target system described in Ref. 3 can be used to enhance \bar{p} collection efficiency. In this system, the proton beam passes through several targets in succession. The \bar{p} 's produced in target i (and other targets upstream) are refocussed on target $(i+1)$ by a lithium lens. Thus, the "image" of all targets are superposed. The capture efficiency is

$$F(Z_{\text{opt}}^{(n)}) \cong \frac{8}{3} n \frac{\epsilon}{\langle \theta^2 \rangle} \frac{\exp(-Z_{\text{opt}}^{(n)} - n/\lambda)}{(\lambda + nZ_{\text{opt}}^{(n)})/\lambda}$$

$$Z_{\text{opt}}^{(n)} \approx \frac{Z_{\text{opt}}^{(1)}}{\sqrt{n}} \approx \frac{1.3\lambda}{\sqrt{n\lambda}} \left(\frac{\epsilon}{\langle \theta^2 \rangle} + \frac{r_p^2}{\epsilon} \right)$$

For $\epsilon = 70 \times 10^{-6}$ m, $p = 6$ GeV, $r_p = 0.5$ mm, $n = 3$, the efficiency gain is about a factor of 2. The antiproton collection angle increases $\sim \sqrt{n} = 1.8$. The lithium lens required must produce a surface magnetic field of 30T.

It should be noted that the same gain could be achieved by pulsing current through a target of length ~ 7 cm, diameter ~ 1 mm, peak (surface) magnetic field 100T. Such a target could only be operated in an explosive mode.

VII.4. Increasing the number of accelerated protons

The cooling time is calculated in Section V.4 (Case B) to be 1.4 sec. This is five times shorter than the cycle time for accelerating protons (7 sec.) in U70. The \bar{p} production process could then be repeated 7 times while the U70 synchrotron remained on flat top at maximum energy (40-70 GeV). The scenario could proceed as follows:

- 1) acceleration of protons for 3 sec. to maximum energy
- 2) production of 4 \bar{p} bunches once each 2 sec;
- 3) cooling and stackings of \bar{p} 's as described above;

Steps 2 and 3 would be repeated 7 times to use all the protons contained in U70. The total cycle time would be increased to ~ 20 sec, and the \bar{p} collection rate would be increased by a factor 2.5, to $N_{\bar{p}} = 1.2 \times 10^8 \bar{p}/\text{sec}$.

VII.5 Increasing Injection Energy for U-70

The efficiency of the antiproton source critically depends on the quality of proton beam accelerated in U-70 (see Section II). It can happen that after commissioning the Booster the beam phase space accelerated in U-70 will be too large, substantially due to perturbations connected with the passage through transition energy. If reduction of these perturbations is impossible, it seems appropriate, for a program of the scale of UNK, to create another Booster with top energy above U-70 transition.

VII.6 Colliding Region for UNK with Low Beta Function

We took, for our luminosity estimations (Section V.7), the minimum beta function value to be 1 m. This is mainly a result of "conventional wisdom". But, obviously, one can discuss beta functions ~ 0.3 m. The necessary lens parameters can be estimated as follows. If we place, at the interaction region, where the "old" (original) value of beta function is β , two quadrupole doublets with distance $2d$ between them, the new value of beta function will be

$$\beta^* = F^2/\beta \quad (7.1)$$

if each doublet has focal length

$$F = d . \quad (7.2)$$

The approximate parameters of these lenses for a low beta section are given in Table 6. For achievement of these parameters the "old" beta function value needs to be increased, as much as possible, at the position of these new doublets (they are turned on after the

beam is accelerated to colliding energy).

One possible way to realize such an optical system is to create and use the lenses with tuned aperture and focal length.

TABLE 6

Parameters of Low Beta Interaction region

Beta functions	0.3 m
Normal beta functions	1 km
Doublet focal length	17.3 m
Distance between doublets	34.6 m
Lens length in doublets	2 m
$\bar{p}(p)$ energy	3 TeV
Lens field gradient	82.5 kG/cm

VII.7 Electron Cooling at Interaction Energy

For achieving high luminosity it is very important to damp the nonlinear bunched beam-beam influence and to exclude other disturbing factors (RF noise, interactions with residual gas, etc.). Any fraction, which can be brought to play on the beam, can have a defining role. Therefore it is extremely important to study the possibility of high energy electron cooling for UNK colliding beams. Application of stochastic cooling for this purpose is not practical because the beam linear intensity is very high and the particle revolution frequency spread is small.

If emittances of the beams, which are being cooled is larger than the cooling electron beam emittance:

$$\varepsilon_e < \varepsilon_p, \varepsilon_{\bar{p}}$$

the cooling time is (10)

$$\tau_{cool}^{-1} = 2 \times 10^2 s$$

(7.3)

with N_e , N_p the number of electrons, protons (antiprotons); β_c the particle velocity; ℓ_b the bunch length; r_e , r_p the classical electron (proton) radius; $L_c \approx 15$ the Coulomb logarithm; η the electron beam circumference ratio; $\Delta\nu_{\max}$ the betatron tune shift due to $\bar{p}p$ collisions; β_{cool} the cooling straight section beta function value; n_b the bunch number. For the parameters

$$\begin{aligned}
 \tau_{\text{cool}} &= 10^3 \text{ sec} \\
 \Delta\nu &= 10^{-2} \\
 N_e &= 10^{12} \\
 \beta_{\text{cool}} &= 1 \text{ cm} \\
 \ell_b &= 1 \text{ m} \\
 \eta &= 10^{-2} \\
 n_b &= 10
 \end{aligned}$$

and with a beta function value in the interaction region, $\beta_{\text{colliding}} = 1 \text{ m}$, the limit is $L = 2 \times 10^{30} \text{ cm}^{-2} \text{ sec}^{-1}$.

The electron beam has to circulate in a special storage ring. The electron energy has to be $E_e = \frac{m}{M} E_p$. Synchrotron radiation cools the electron beam. Quantum fluctuations and intrabeam scattering processes will define the electron beam emittance and its momentum spread. If the condition $\varepsilon_e < \varepsilon_p$ is not satisfied the cooling efficiency will be very much decreased. This can be compensated for by the addition of strong electron focusing in the cooling region ($\beta_e \ll \ell_{\text{cool}}$) with a necessary optimization of the focusing structure of the electron storage ring.

VIII Comparison of Antiproton Sources

The comparison of design parameters for the \bar{p} sources of CERN, FNAL, and IHEP is given below.

Table 7

Laboratory	CERN	FNAL	IHEP
1. Proton Beam Parameters			
Energy (GeV)	28	80	70
Protons/cycle	1×10^{13}	1.8×10^{13}	6.6×10^{12}
Cycle duration (sec)	2.6	10	7
2. Antiproton Beam Parameters			
Antiproton momentum on target (GeV/c)	3.5	5.5	5.5
Beam emittance (μm)	100	5	60
Momentum spread	$\pm 0.75\%$	$\pm 1\%$	$\pm 3.2\%$
\bar{p} /cycle	$2.5 \cdot 10^7$	$2.5 \cdot 10^7$	$3.2 \cdot 10^8$
Accumulation rate (sec^{-1})	$1 \cdot 10^7$	$2 \cdot 10^6$	$4.7 \cdot 10^7$

IX. Antideuteron Accumulation

The proposed scheme for the \bar{p} source is available, practically without change, for accumulation of antideuterons and antinucleons. The diminution of accumulation rate for antideuterons will be about a factor 10^4 .

Along with antideuterons, other particles with negative charge and the same momentum, will be accepted in deceleration from the target. A pure antideuteron beam can be obtained if we use an "antideuteron tuned" RF system and a specific magnetic field so that nonequilibrium (parasitic) particles will be lost to the walls.

For antideuteron accumulation primary stochastic cooling will be very effective, because the antideuteron number per cycle is very small. This means that all the protons from U-70 can be used for antideuteron production because now there is not a strong limitation on particle bunch length in the decelerator (no RF rotation!). Also, the whole acceptance of the decelerator can be filled.

The antideuteron accumulation scenario with primary stochastic cooling is as follows:

1. Proton acceleration to 70 GeV in U-70.
2. Adiabatic switching off of 30th harmonic RF in U-70 and beam debunching.
3. Adiabatic switching on of fast harmonic RF, and formation of a single bunch.
4. RF rotation of the proton bunch to achieve a bunch length equal to the decelerator circumference (by fast switch on of first harmonic RF at large voltage).

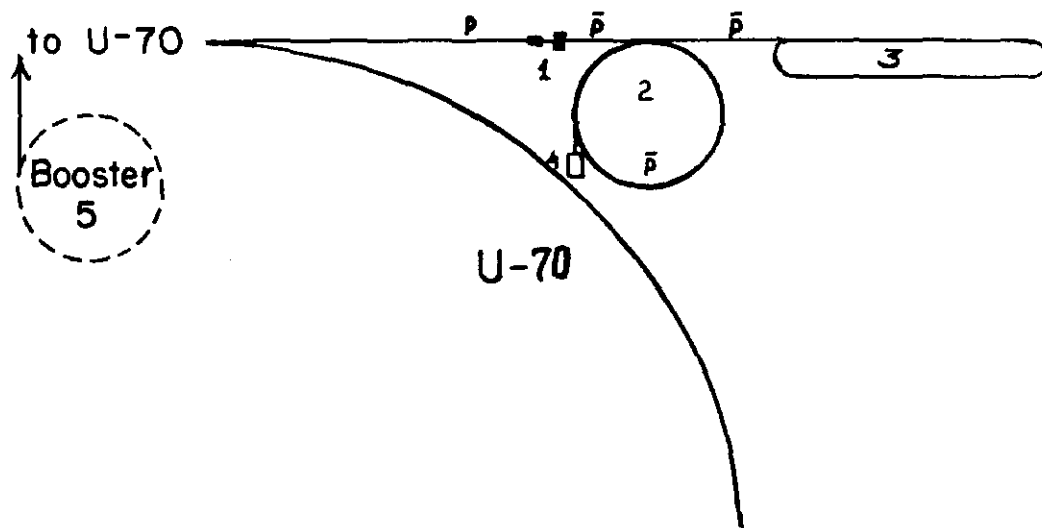


Fig. 1 The \bar{p} source plan.
 1. Target, 2. Synchrotron-decelerator,
 3. Cooler-accumulator,
 4. Special proton linear injector
 (see V.8), 5. U-70 Booster

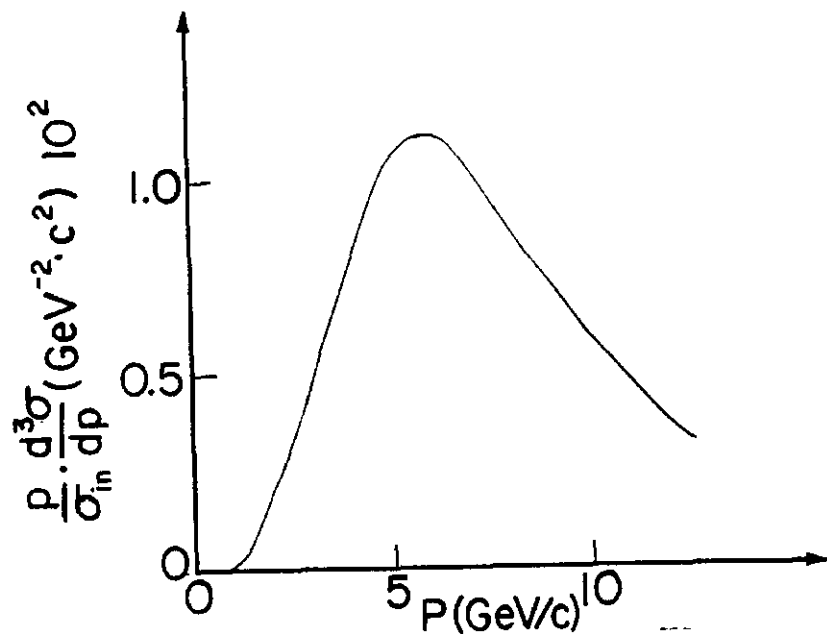


Fig. 2 Cross section of antiproton production per interacting proton for 70 GeV proton energy (result of Ref^{5,6} with symmetric reflection of values about $Y_F, pp = 0$).

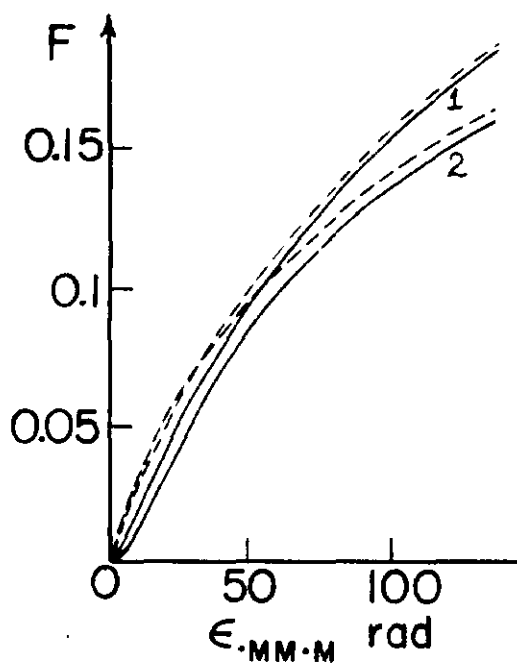


Fig. 3 Dependence of F on ϵ .
 Proton momentum, 76 GeV/c
 \bar{p} momentum, 6 GeV/c
 proton beam radius in target:
 $r_0 = 0$ (-----)
 $r_0 = 0.045$ (————)

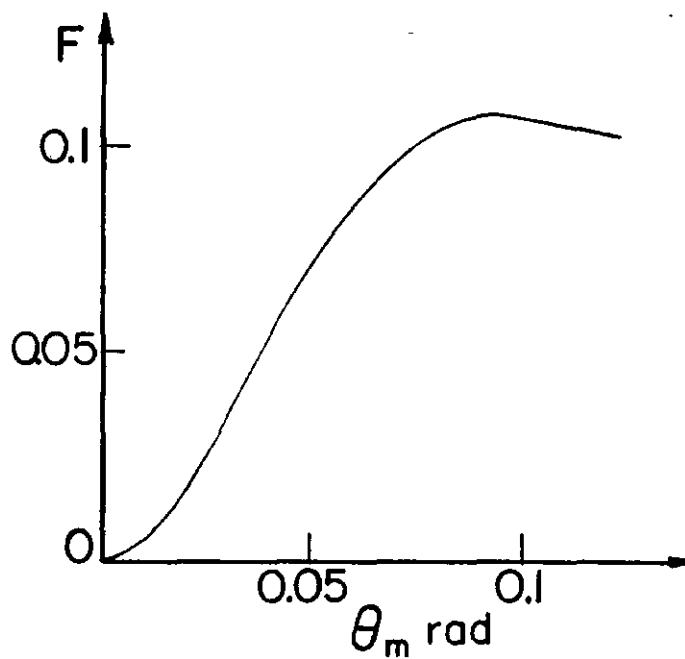


Fig. 4 Dependence of F on \bar{p} capture angle θ_m . Target length has its optimum value, and $\epsilon = 70 \text{ mm} \cdot \text{mrad}$.

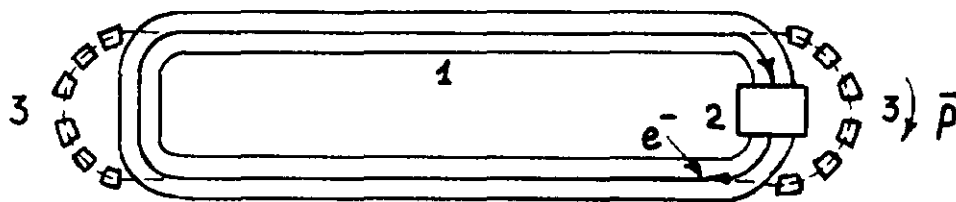


Fig. 5 The cooler-accumulator plan.
1. Solenoid with longitudinal magnetic field.
2. Electron gun and collector
3. Antiproton bending magnet channel.

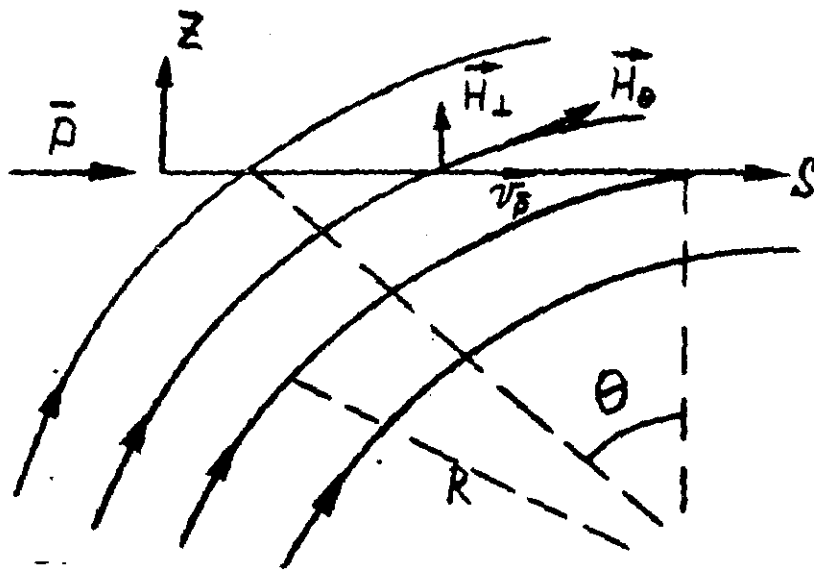
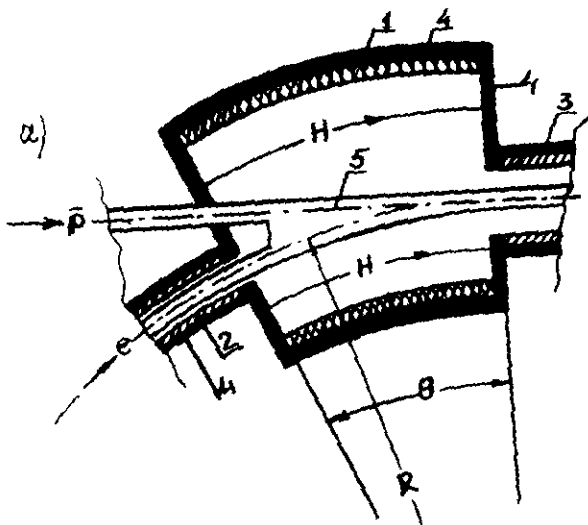


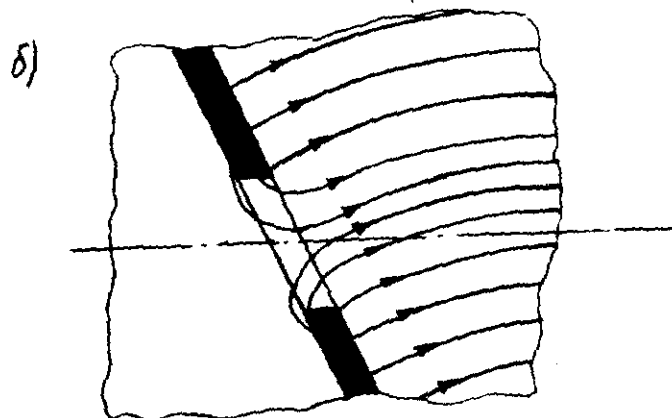
Fig. 6 Trajectory of antiprotons and geometry of the magnetic fields in the cooler toroid region.

Fig. 7 Injection of antiprotons and electrons into the cooling section.

- A. Layout of electron guide field and accompanying flux return steel
1. Large toroidal solenoid
 2. Small toroidal solenoid
 3. Long straight solenoid
 4. Flux return
 5. Vacuum Chamber



B. Magnetic flux lines near interface



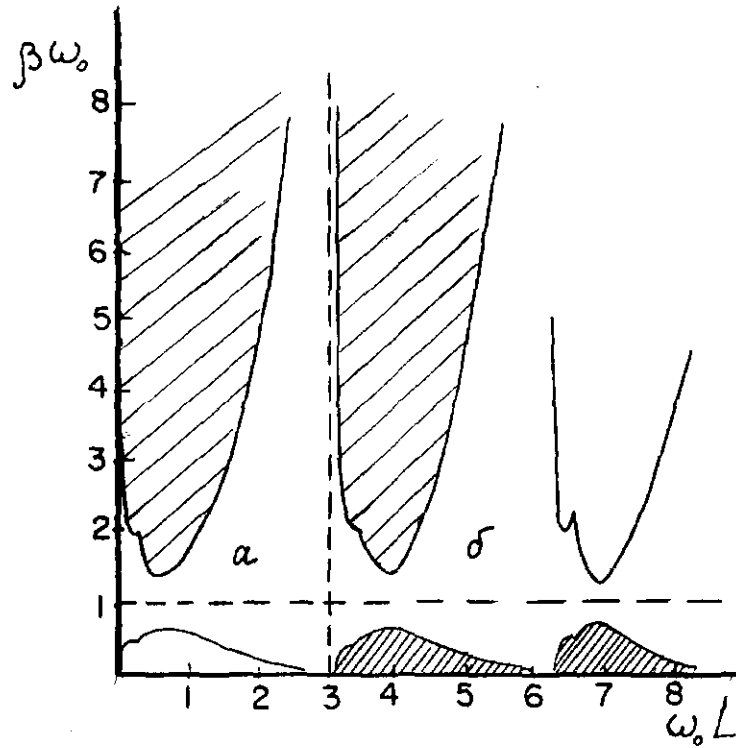


Fig. 7 Regions of betatron oscillation stability, as given in section (V.5). β is the beta function at the cooling section entrance; L the section length; ω_0 is given by (5.11). Instability regions are shaded. a is the unneutralized case; b the neutralized one.

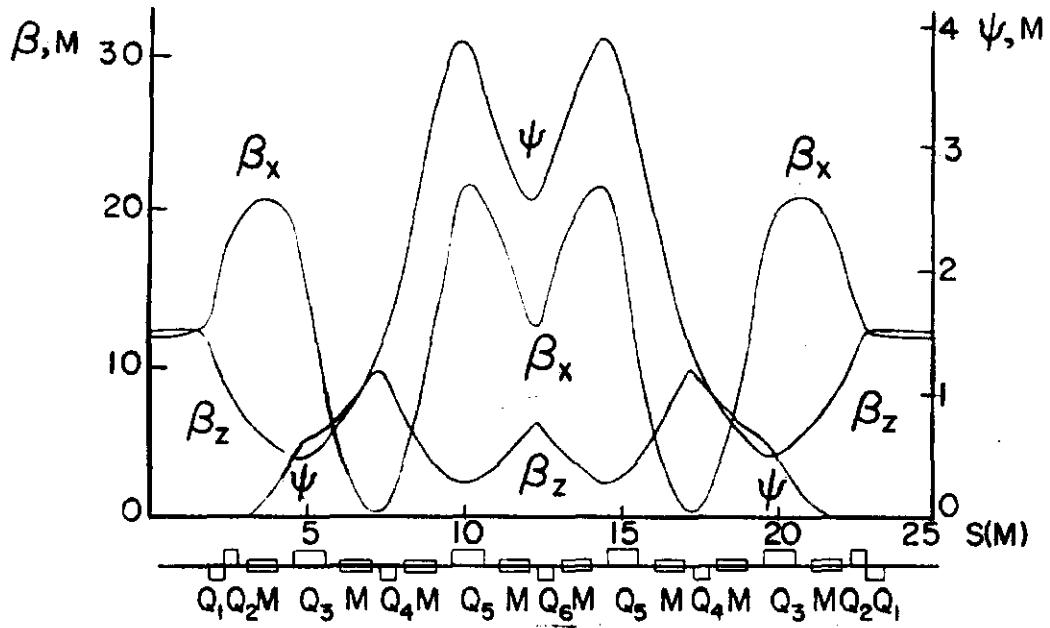


Fig. 8 Betatron and dispersion functions for half rings on cooler. Here $Q_1 - Q_6$ are quadrupoles, M - bending magnets.

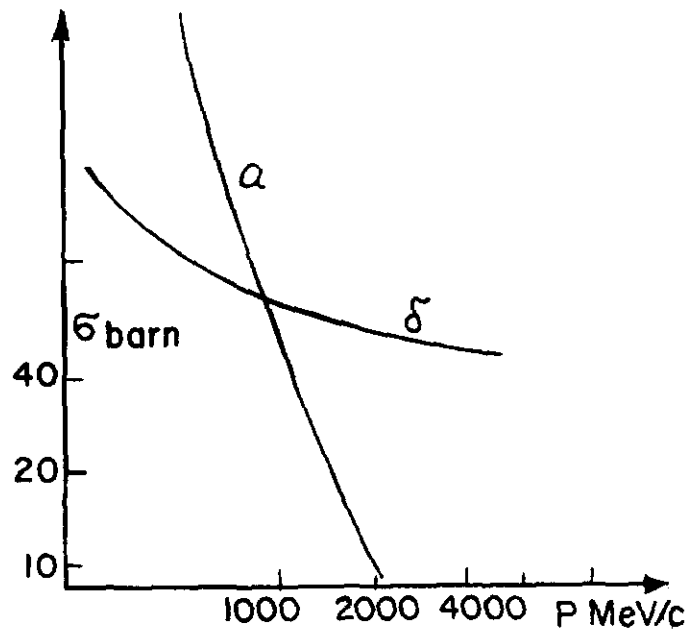


Fig. 9 The dependence of single scattering and nuclear absorption cross sections on p momentum.

a. Single scattering, for $\theta_{\max} = 3$ mrad.

b. Nuclear absorption

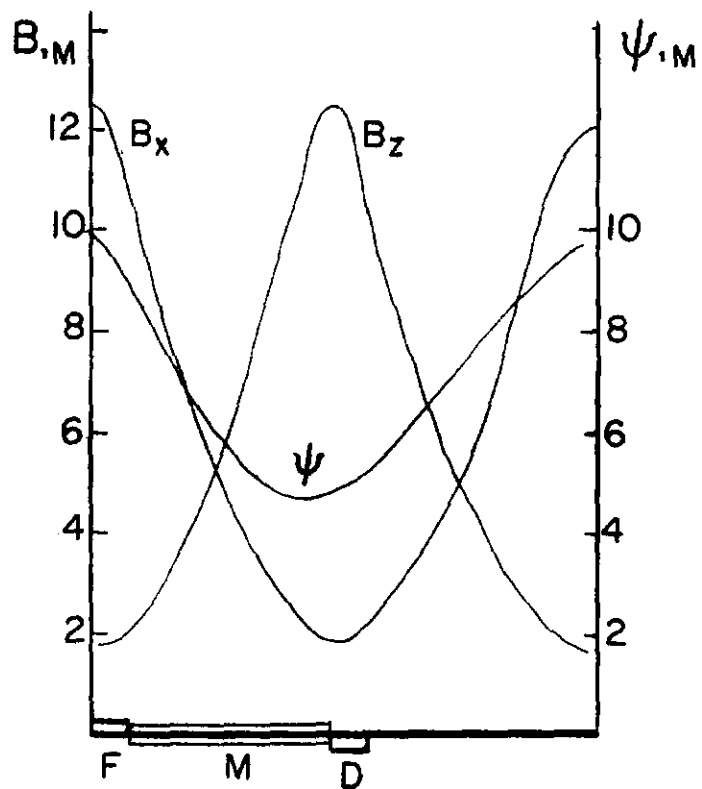


Fig. 10 Betatron and dispersion functions for the decelerator, with periodicity elements. FMD: F - focusing quad., D - defocusing quad. (lengths = 0.5 m), M - bending magnets.

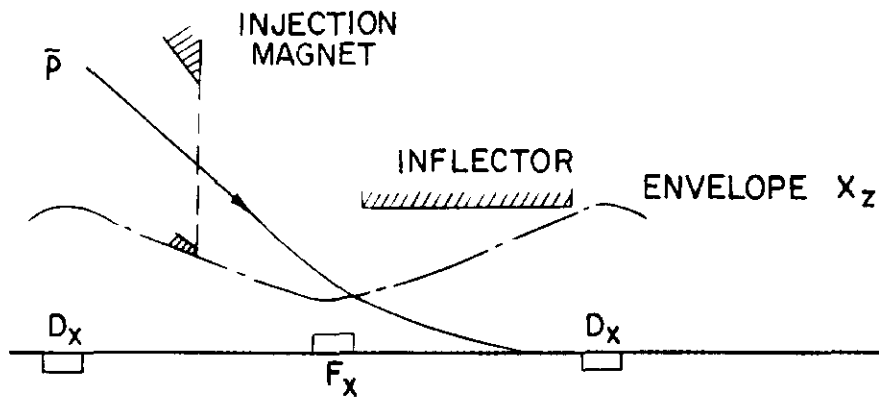


Fig. 11 Arrangement of injection into the synchrotron decelerator.

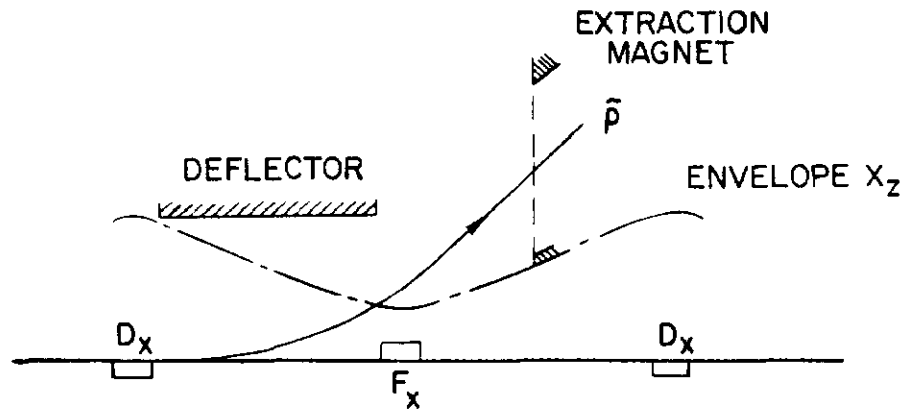


Fig. 12 Arrangement of extraction from the synchrotron decelerator.

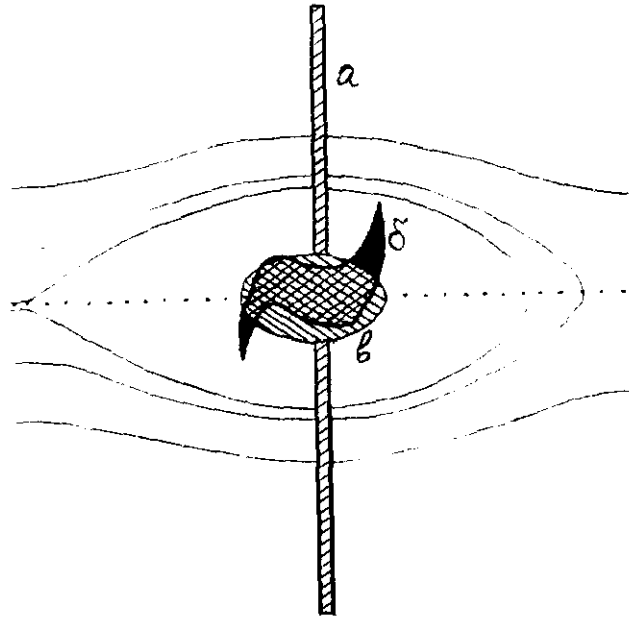


Fig. 13 Antiproton longitudinal phase space capture in decelerator, a, at injection, before rotation; b, after rotation; c, area available for cooling after deceleration; d, 4th harmonic separatrix.

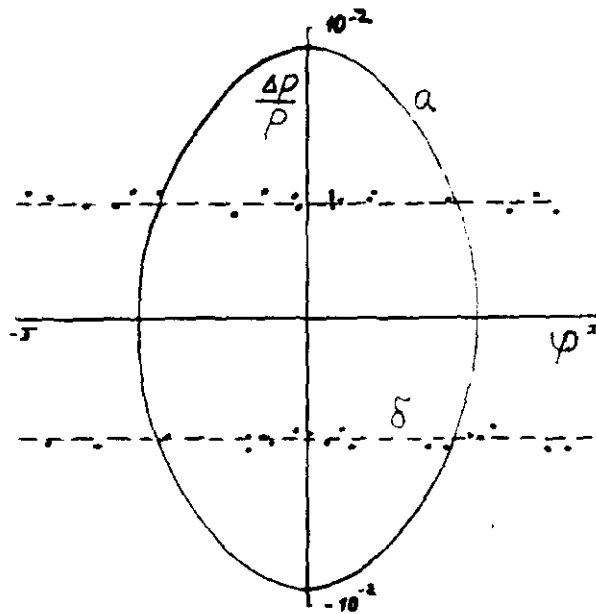


Fig. 14 Adiabatic debunching of \bar{p} beam
 a - \bar{p} longitudinal area after deceleration
 b - after slow (~ 10 msec) switch off of RF.

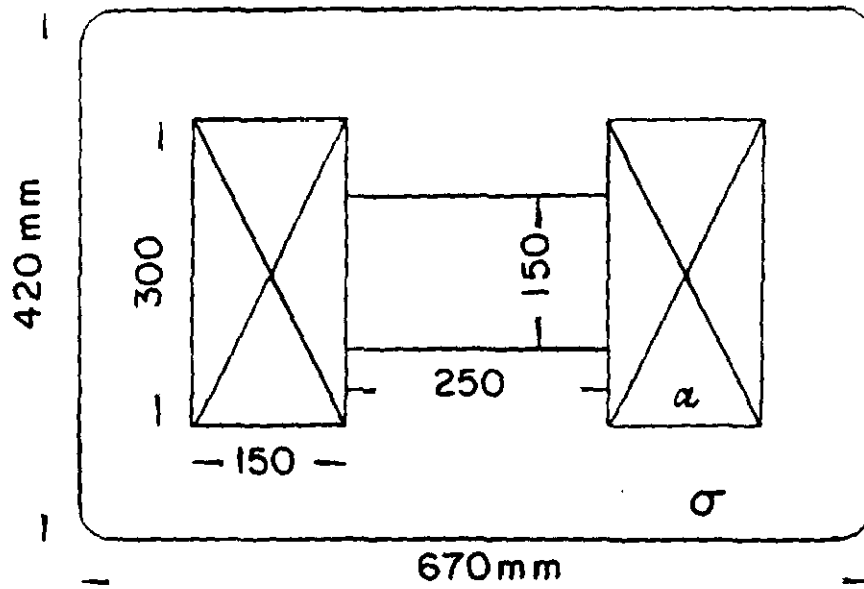


Fig. 15 Magnet cross section for
 the decelerator synchrotron.
 a - coils , b - flux return yolk

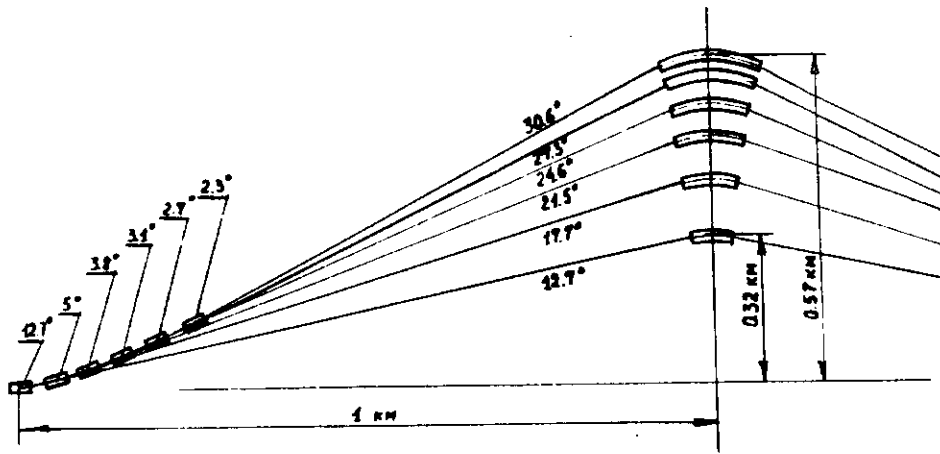


Fig. 16 The delay channels

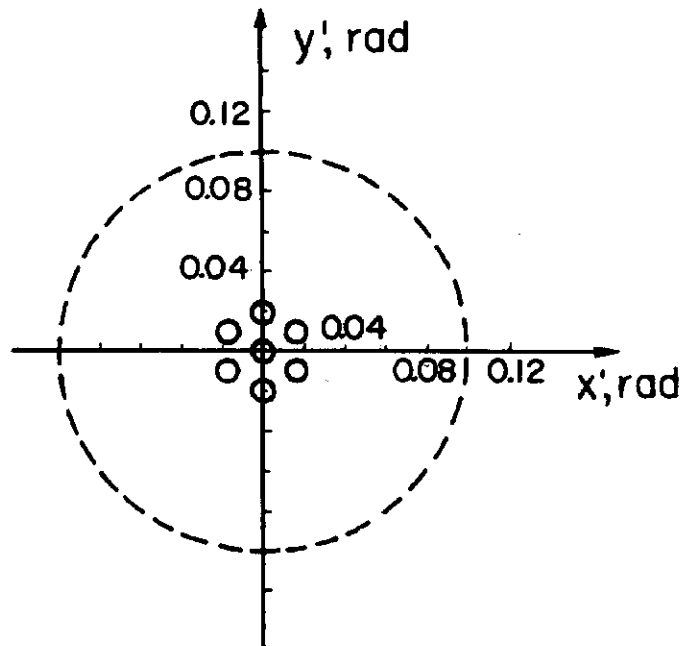


Fig. 17 Scheme of proton bunch focusing at the target center plane. Dotted curve gives angular acceptance.

5. Single turn beam extraction, antideuteron injection in the decelerator with antideuteron energy about 5 GeV.
6. Stochastic cooling - transverse and longitudinal.
7. Antideuteron deceleration to 226 MeV (0.95 GeV/c momentum).
8. Extraction and injection in the accumulator, electron cooling and stacking.

Let us estimate the antideuteron accumulation rate for the simplest case, where the antideuteron momentum at cooling is the same as for antiprotons (954 MeV/c). If the electron current density is also, as for case B (section V.4) $j_e = 1.5 \text{ A/cm}^2$, the accumulator lattice can have the same field and only the electron energy must be decreased in 61.5 keV.

For maximum accumulation rate we need to have $\epsilon \cdot \Delta p/p$ maximal, which means that 2/3 of the decelerator aperture has to be devoted to beam betatron emittance width, and 1/3 for momentum dispersion width. From Fig. 10 and table 3 we find the emittance and momentum spread of an antideuteron beam which can be accepted from target to completely fill the decelerator (table 8).

Before deceleration the antideuteron beam has to be cooled with stochastic cooling so that its size after deceleration will not be larger than the aperture and its emittance and momentum spread will be matched to the electron cooling (section V.4 case B). The antideuteron beam parameters before cooling are determined by the decelerator and accumulator acceptances ($360 \pi \text{ mm.mrad}$). This dictates the stochastic cooling requirements: before deceleration the beam

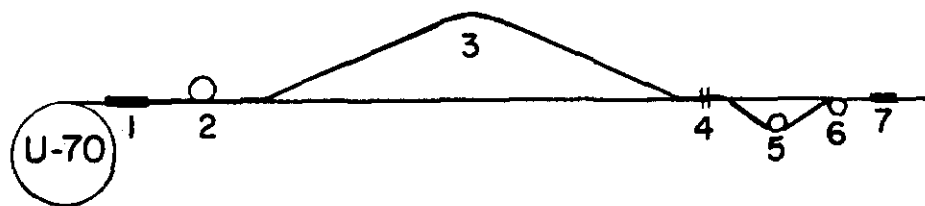


Fig. 18 Plan for improved antiproton source.

1. Monochromating target; 2. Buncher;
3. Delay channels; 4. Target station
5. Monochromating synchrotron;
6. Decelerator synchrotron;
7. Accumulator

emittance and momentum spread have to be reduced about 6 times (in momentum spread). Without stochastic cooling the accumulation rate for antideuterons would be about $7.3 \times 10^3 \text{ sec}^{-1}$, i.e. 8 times less.

Table 8

ANTI DEUTERON BEAM ACCUMULATION

A. Injection

Antideuteron momentum	5.5 GeV/c
Beam emittance	210 mm.mrad
Beam momentum spread	$\pm 2.5\%$

B. After Stochastic Cooling

Emittance	60 mm.mrad
Momentum spread	$\pm 0.08\%$

C. After Deceleration

Antideuteron energy	226 MeV
momentum	954 MeV
Beam emittance	360 mm.mrad
Electron cooling time	0.15 sec.
Antideuteron number per cycle	2×10^5
Accumulation rate	$2.8 \times 10^4/\text{sec}$

The cooling time for these parameters is significantly less than the cycle duration. This means that "case B" is much less optimal than it was with antiprotons. Further optimization (transforming towards "case C") is a subject for future work.

REFERENCES

1. G. I. Budker, A. N. Skrinsky, "Uspekhi Physicheskich Nauk", V. 124, N4, 1978.
2. Colliding Beam Proposal for Fermilab. "In Proceed. of V Sov. Nation. Conf. on Particle Accelerators". V. II, p. 306, Dubna, 1976.
P. McIntyre, et al., Fermilab Report TM-689-2000, 1976.
3. G. I. Budker, et al. In Proceed. of V Sov. Nation. Conf. on Particle Accelerators, V. II, p. 299, Dubna, 1976.
4. VAPP-NAP group report. In Proceed. of VIII Intern. Conf. on Particle Accelerators, Geneva, CERN, p. 72, 1971.
5. F. Binon, et al., Phys. Letter. V. 30B, 506, 1969.
6. Yu. M. Antipov, et al., Phys. Letter. V. 37B, 165, 1971.
7. V. I. Kudelainen, et al., Preprint INP 72-70, Novosibirsk, 1970; CERN Yellow Report 77-08, Geneva, 1977.
8. V. I. Kudelainen, et al., "Journal of Techn. Physics" (Sov.) V. 76, N8, 1678, 1976.
9. B. Autin, CERN/PS/AA/79-18, 1979.
10. Ya. S. Derbenev, A. N. Skrinsky, "On High Energy Electron Cooling", INP Preprint 79-87, Novosibirsk, 1979.
11. V. I. Balbekov, et al., "Unk IHEP" Preprint, IHEP-OUNK 79-134, Serpukhov, 1978.
12. G. I. Budker, et al. In Proceed. of IInd Nation. Conf. on Particle Accel., Moskow, Nauka, 1972, V. II, p. 196.

13. H. Koziol, "Antiproton Accumulator Parameter List", 8th edition, CERN, September 1979.
14. Antiproton Source. Fermilab, October 1979.
15. Low Energy Hadron Production at Zero Angle in Proton Nucleus Collisions at 70 GeV, IHEP-INP Collaboration, IHEP Preprint 81-107, Serpukov (1981).